https://ntrs.nasa.gov/search.jsp?R=19840013833 2020-03-21T00:01:58+00:00Z

NASA
TP
2298
c.1

TECH LIBRARY KAFB, NM
0067890

NASA
Technical
Paper
2298

April 1984

Survey of NASA Research on Crash Dynamics

Robert G. Thomson,
Huey D. Carden,
and Robert J. Hayduk

LOAN COPY: RETURN TO
AFWL TECHNICAL LIBRARY
KIRTLAND AFB, N.M. 87117

NASA

TECH LIBRARY KAFB, NM
0067890

NASA
Technical
Paper
2298

1984

Survey of NASA Research on Crash Dynamics

Robert G. Thomson,
Huey D. Carden,
and Robert J. Hayduk

Langley Research Center
Hampton, Virginia

NASA
National Aeronautics
and Space Administration

**Scientific and Technical
Information Office**

SUMMARY

Ten years of structural crash dynamics research activities conducted on general aviation aircraft by the National Aeronautics and Space Administration (NASA) are described. Thirty-two full-scale crash tests were performed at Langley Research Center, and pertinent data on airframe and seat behavior were obtained. Concurrent with the experimental program, analytical methods were developed to help predict structural behavior during impact. The report includes experimental and analytical correlations of load-limiting subfloor and seat configurations tested statically and dynamically. Also included is an assessment of the effects of flight parameters at impact on cabin deceleration pulses at the seat/occupant interface, load-limiting subfloor and seat configuration studies, airplane section testing for computer modeling validation, and emergency-locator-transmitter (ELT) investigations to determine probable cause of false alarms and nonactivations. Computer programs were developed to provide designers with methods for predicting accelerations, velocities, and displacements of collapsing structures. Tests on typical full-scale aircraft and aircraft components were performed to verify the analyses and to demonstrate load attenuating concepts.

INTRODUCTION

Aviation crash dynamics research has a history (fig. 1) dating back to the pioneering work of Hugh De Haven in the 1940's. Having survived a midair collision and the ensuing crash that caused three deaths, De Haven initiated research into crashworthiness involving on-site investigations of airplane accidents to identify components and/or subsystems contributing to injuries and/or fatalities. Results from this research produced design guidelines that are still pertinent (ref. 1). The Ag-1 crop-dusting airplane, built by Fred Weick at Texas A&M College, incorporated a number of original crashworthy (CW) features based on principles espoused by De Haven (refs. 2 and 3). These features are still found in production agricultural airplanes.

Another milestone in the progress of improved structural crashworthiness of aircraft is the first series of aircraft crash/fire tests conducted by the National Advisory Committee for Aeronautics (NACA) at the Lewis Research Center in 1952. These tests identified mechanisms which initiate postcrash aircraft fires (ref. 4). In 1964, the Federal Aviation Administration (FAA) conducted two full-scale crash tests of transport airplanes at the Flight Safety Foundation facility in Phoenix, Arizona. One of these tests involved a McDonnell Douglas DC-7 and the other a Lockheed L-1649. The objectives of these tests were (1) to obtain crash environmental data, (2) to study fuel containment, and (3) to collect data on the behavior of various components and equipment aboard the airplane (refs. 5 and 6). After a 20-year hiatus, the FAA is proposing another full-scale transport crash test to be conducted in cooperation with NASA. This proposal involves crashing a remotely piloted Boeing 720 into the ground to simulate a survivable crash landing.

Since the late 1950's, the U.S. Army has been investigating aircraft accidents, studying crash injuries, and conducting crashworthy research (fig. 1). These efforts culminated in the Crash Survival Design Guide first published in 1967 and revised in

1969 (ref. 7). The Design Guide is used as a tool for aircraft engineers and designers and represents a major milestone toward improved crashworthiness in military aircraft. By requiring that Army aircraft be built to the Design Guide requirements, helicopter crash fires have been virtually eliminated, and the overall crashworthiness of the Army aircraft fleet has been substantially improved. The Army Flight Safety and Helicopter Crash Testing Program (fig. 1) validated selected crashworthy design concepts (ref. 8). Army interest in crashworthiness continues, and the Design Guide was recently updated on the basis of the latest research results. In addition, a crashworthy utility helicopter (Black Hawk) has been put into production, and production of a crashworthy attack helicopter is imminent (refs. 9 and 10).

Advanced materials, in particular graphite-epoxy composites, are being considered by the Army for future helicopter weight-saving designs. The Army has embarked on a program to build an all-composite airframe helicopter, which still requires that the crashworthy requirements applicable to metal aircraft be applied in the design stage (ref. 11).

In 1972, NASA embarked on a cooperative effort with FAA and industry to develop technology for improved crashworthiness in general aviation airplanes. The effort included analytical and experimental structural concept development and involved full-scale crash testing (ref. 12). Prior to 1972, little full-scale crash testing of general aviation airplanes had been done, except for some high-wing, single-engine tests performed by NACA in 1952 and a crash test program involving two twin-engine airplanes performed by Aviation Safety Engineering and Research (AVSER) in 1964-65 for the U.S. Army. (See refs. 13 and 14). The Langley full-scale, free-flight crash simulations examined the response of the airplane structure, seats, and anthropomorphic dummies to realistic crash deceleration pulses. Definitive data that cannot be obtained by investigating field accidents, such as the impact attitude and velocity, crash forces, and dummy accelerations, were obtained in these crash tests.

The general aviation crash dynamics program is being completed, and attention is being focused on commercial transport airplanes. It is recognized that there are significantly fewer numbers of accidents of transport airplanes than of either general aviation airplanes or military helicopters, nevertheless the introduction of the wide-body jumbo jet with passenger complements of 300 to 400 presents the potential for substantial loss of life or injuries in a single accident. Further, the use of new advanced materials dictates that efforts continue in safety research to enhance occupant survivability in the event of a crash. With the continued technical advances in analytical predictive methods and experimental methods, many tools are becoming available for use by the aircraft designer in addressing the crash response characteristics of future aircraft.

The purpose of this report is to highlight the research activities in crash dynamics that have been actively pursued at the Langley Research Center for the past 10 years; these include full-scale crash testing; seat, occupant, and restraint system simulation; load attenuating subfloor and seat concepts; and emergency-locator-transmitter activation studies.

SYMBOLS

F force

f frequency

g	acceleration due to gravity
k	spring constant
m	mass
s	slide-out distance
t	time
Δt	pulse duration
V	velocity of airplane
ΔV	change in velocity
$\ddot{X}_a$	longitudinal deceleration in airplane X_a-axis, $\ddot{x}_a/g$, g units
$\ddot{X}_{a,max}$	maximum longitudinal deceleration, g units
$\ddot{x}_a$	longitudinal deceleration in airplane x_a-axis
Z	normal (vertical) gravity axis
$\ddot{Z}$	vertical input acceleration
$\ddot{Z}_a$	normal (vertical) deceleration in airplane Z_a-axis, $\ddot{z}_a/g$, g units
$\ddot{Z}_{a,max}$	maximum normal deceleration, g units
$\ddot{z}_a$	normal (vertical) deceleration in airplane z_a-axis
γ	flight-path angle of airplane at impact
δ	displacement
ζ	damping ratio
θ	pitch angle of airplane at impact
μ	coefficient of friction
ω	natural frequency

Subscripts:

fp	flight path
max	maximum
p	peak
Z	Z-axis in gravity system

1 associated with major longitudinal impact

2 associated with slide-out distance

Abbreviations:

Accel	acceleration
CW	crashworthy
c.g.	center of gravity
DOF	degrees of freedom
DRI	dynamic response index
E/A	energy absorber
ELT	emergency locator transmitter
FAA	Federal Aviation Administration
F.S.	fuselage station
GA	general aviation
LaRC	Langley Research Center

FULL-SCALE CRASH TESTING

Full-scale crash testing is performed at the Langley Impact Dynamics Research Facility shown in figure 2. This facility is the former Lunar Landing Research Facility modified for free-flight crash testing of full-scale aircraft structures and structural components under controlled test conditions (ref. 15). The basic gantry structure is 73 m (240 ft) high and 122 m (400 ft) long and is supported by three sets of inclined legs spread 81 m (267 ft) apart at the ground and 20 m (67 ft) apart at the 66-m (218-ft) level. A movable bridge with a pullback winch for raising the test specimen spans the top and traverses the length of the gantry.

Test Method

The aircraft is suspended from the top of the gantry by two swing cables and is drawn back above the impact surface by a pullback cable. An umbilical cable used for data acquisition is also suspended from the top of the gantry and connects to the top of the aircraft. The test sequence is initiated when the aircraft is released from the pullback cable to permit the aircraft to swing pendulum style onto the impact surface as shown schematically in figure 3. The swing cables are separated from the aircraft by explosive devices just prior to impact to free it from restraint. The umbilical cable remains attached to the aircraft for data acquisition, but it also separates by explosive devices before it becomes taut during slide-out. The separation point is held relatively fixed near the impact surface, and the flight-path angle is adjusted from 0° to 45° by changing the length of the swing cable. The height of the aircraft above the impact surface at release determines the impact

velocity, which can be varied up to 26.8 m/sec (60 mph). The movable bridge allows the pullback point to be positioned along the gantry to insure that the pullback cables pass through the center of gravity and act at 90° to the swing cables.

To obtain flight-path velocities in excess of 26.8 m/sec (60 mph), a velocity augmentation method was devised which used wing-mounted rockets to accelerate the test specimen on its downward swing. Two or more Falcon rockets were mounted symmetrically at each engine nacelle location and provided a total thrust of up to 77 850 N (17 500 lbf). The aircraft is released after rocket ignition. The rockets burn during most of the downward acceleration trajectory but burnout prior to impact. The velocity augmentation method provides flight-path velocities of 26.8 to 44.7 m/sec (60 to 100 mph) depending upon the number and burn time of the rockets.

Instrumentation

Data acquisition from full-scale crash tests is accomplished with onboard strain gages and accelerometers, and with extensive photographic coverage with low-, medium-, and high-speed cameras both interior and exterior to the aircraft. The location and frame rate of the cameras are discussed in detail in reference 15. The strain-gage accelerometers (range of 250g and 750g at 0 to 2000 Hz) are the primary data-generating instruments and are positioned at various locations in the fuselage to measure accelerations in the normal, longitudinal, and transverse directions to the aircraft axis. Instrumented anthropomorphic dummies (National Highway Traffic Safety Administration 50th percentile, Hybrid II, Part 572, ref. 7) were onboard for all full-scale aircraft tests conducted at Langley. The dummy restraint system arrangement and type of restraint varied from test to test.

Correlation of Crash Data With Flight Parameters at Impact

Langley crash test data.- A typical twin-engine, general aviation airplane crash test is shown in figure 4 at impact for a flight-path angle of -30°, a pitch angle of -30°, and an impact velocity of 26.8 m/sec (60 mph). A photographic sequence of this test is illustrated in figure 5. Figure 5(b) shows conditions just prior to impact followed in figure 5(c) by crushing of the nose radome. (See also fig. 4.) The photograph in figure 5(d) shows the engine making contact and digging into the impact surface. The initial movement of the dummy occupant, as seen through the window (but not readily visible in this sequence), occurs in figure 5(d). Shown in figure 5(e) are the wing tips lying flat on the impact surface and the cabin deformation, which resulted in the window breakage adjacent to the first passenger and the door popping open. Figure 5(h) shows the slapdown of the aft cabin section with pronounced skin buckling behind the door. Typical normal- and longitudinal-deceleration pulse shapes (with triangle approximations), similar to those in figure 6, were noted for this -30° test as well as for numerous other general aviation airplane crash tests conducted in the crash dynamics program (refs. 16 through 22).

Other crash test data.- Representative decelerations for a transport airplane and a fighter airplane are shown in figures 7(a) and (b), respectively (refs. 23 through 25). The same triangular-deceleration pulse is noted in these airplane crash tests as in the general aviation airplanes; however, the duration of the pulses is generally longer as a result of the higher velocities and greater structural crushing distances available to dissipate the impact energy. Durations are basically between 0.15 and 0.3 sec as compared with 0.15 sec or less for the general aviation airplane (refs. 20 and 21). The data from the controlled crash tests of these various air-

planes are summarized in table I . The flight-path angle, pitch angle, and flight-path velocity are given for each test. The nominal values of the roll and yaw angles (not included) were essentially zero with the exception of tests 9, 10, FAA-2, and FAA-3, which were tests with planned roll and/or yaw angles. Also presented in table I are the experimental normal and longitudinal pulse data (i.e., maximum deceleration, pulse duration, velocity change, and impulse). Calculated impulse and velocity changes are included for the normal direction pulse data.

Impulse calculations.- The calculated impulse and velocity changes for both normal and longitudinal directions were obtained from expressions derived from a simplified analysis of the complex crash scenario based on impulse-momentum relationships (ref. 26). Assumptions were made which uncoupled the analytical expressions for the normal and longitudinal airplane impulses. These impulses were expressed in terms of flight-path velocity V_{fp}, pitch angle θ, flight-path angle γ, and acceleration of gravity g as follows:

For the normal crash pulse approximation

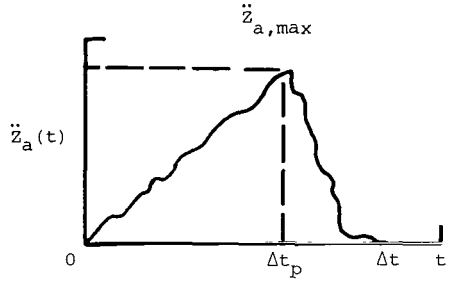

the impulse-momentum relationship is

$$\int_0^{\Delta t} F_Z(t)\,dt = \frac{mg\ddot{z}_{a,max}}{\cos\theta}\left[\int_0^{\Delta t_p} \frac{t}{\Delta t_p}\,dt + \int_{\Delta t_p}^{\Delta t} \frac{\Delta t - t}{\Delta t - \Delta t_p}\,dt\right] = m\,\Delta V_Z$$

and when integrated and simplified is

$$\ddot{z}_{a,max}\,\Delta t = \frac{2V_{fp}}{g}\sin\gamma\cos\theta$$

For the longitudinal crash pulse approximation

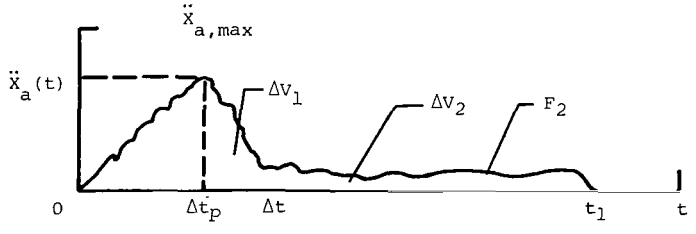

the impulse-momentum relationship is

$$\int_0^{\Delta t} F_Z(t)\,dt = \frac{mg\ddot{x}_{a,max}}{\sin\theta}\left[\int_0^{\Delta t_p} \frac{t}{\Delta t_p}\,dt + \int_{\Delta t_p}^{\Delta t} \frac{\Delta t - t}{\Delta t - \Delta t_p}\,dt\right] = m\,\Delta V_1$$

and when integrated and simplified is

$$\ddot{x}_{a,max}\,\Delta t = \frac{2}{g\cos\theta}\left(V_{fp}\cos\gamma - \sqrt{2g\mu s}\right)$$

Crash deceleration pulse data from table I are plotted in figure 8 for comparison with the simplified analysis.

Figure 8 shows normal impulse $\ddot{z}_{a,max}\,\Delta t$ plotted as a function of the vertical change in velocity on a log-log scale. Lines on the chart represent analytical results for three assumed crash impulse shapes: a triangular shape, a half-sine wave shape, and a rectangular wave shape. Symbols represent experimental data. Experimental results cluster near the line for an assumed triangular-deceleration pulse. The lower cluster ($\ddot{z}_{a,max}\,\Delta t \approx 1.5$) is data for general aviation tests at a flight-path angle γ of -15°. The middle cluster ($\ddot{z}_{a,max}\,\Delta t \approx 2.5$) is data for general aviation tests at a flight-path angle γ of -30°. The upper cluster ($\ddot{z}_{a,max}\,\Delta t \approx 4.5$) is data for transport and fighter tests. The general aviation crash tests, with the exception of two tests into dirt, were onto a concrete surface, whereas the transport tests were into a dirt embankment. In spite of these differences, the crash pulse data correlate reasonably well with the analytical prediction for the triangular pulse assumption.

Figure 9 presents the longitudinal impulse $\ddot{x}_{a,max}\,\Delta t$ plotted against the velocity change parallel to the airplane longitudinal axis, which is expressed in terms of the impact velocity and slide-out parameters. Analytical curves are shown in the figure for a triangular-deceleration pulse, a half-sine pulse, and a rectangular pulse. Although the longitudinal-pulse data in figure 9 show somewhat greater scatter than the crash data normal to the airplane (fig. 8), the trend is basically along the analytical curve for the triangular pulse shape with some data near the half-sine analytical curve. As was true for the crash data normal to the airplane, the longitudinal data obtained from the transport crash tests into the dirt embankments also fall on the same analytical curve as the general aviation crash test results. Note that the range of agreement between the analytical and experimental longitudinal crash data involves at least an order of magnitude on both the velocity change and impulse scales.

Slide-out distance.- The horizontal slide-out distance following the major impact is a parameter of importance in assessing the longitudinal-impulse data. Slide-out distances were determined for most of the NASA data. The velocity change ΔV_2 which occurred during the slide-out is presented in figure 10 as a function of the slide-out distance. The ΔV_2 values were determined from the known flight-path velocity and the measured ΔV_1 values during the major impact. As shown in figure 10, the bulk of the slide-out distances lies along the line for $\mu = 0.42$. Several low data points are the result of the airplane sliding only on the nose structure and rolling on the main gear during the slide-out period. The average

value of μ of approximately 0.42 includes slide-out distances on concrete, asphalt, and grassy surfaces (gear retracted or broken off).

Applications.- The crash test parameters included in these data do not encompass all crash scenarios. However, the data are believed to adequately represent the serious but potentially survivable general aviation airplane crash situation. These data can be useful in a number of applications wherein either reasonable estimates can be made of the magnitude and duration of a crash pulse from postcrash analysis or flight parameters at impact can be assumed from which the various impulse-momentum relationships can be evaluated. For instance, it is frequently possible to obtain reasonable estimates of a number of crash parameters (in the absence of flight recorder data) by examining the crash site and the airplane involved. An assessment of the damage pattern and crushing of the airplane can indicate the most probable impact attitude such as flight-path angle and pitch angle. An evaluation of the crush pattern transferred to a figure which has station reference lines may also give estimated flight-path angle and pitch angle as well as the structural crush distance. Probable impact velocity can be assumed and a measurement of the slide-out distance can be made. With this information and the impulse-momentum relationships, reasonable values of a number of crash parameters can be calculated. (See refs. 26 and 27.) For assumed flight parameters at impact, either $\ddot{Z}$ can be calculated for various assumed crush distances, or conversely, for an assumed or desirable $\ddot{Z}$ the required effective crush distance can be computed. For longitudinal decelerations, the effects of various velocity changes on the slide-out distance can be determined.

Human tolerance considerations.- Interpretation of the experimental and analytical results for the crash data should involve human tolerance considerations. (See ref. 28). In Eiband curves (ref. 29) for human tolerance, pertinent human and animal experiments applicable to impact forces were analyzed, compared, and presented on the basis of a trapezoidal pulse. For example, figure 11 presents the maximum magnitude and time duration limits for headward accelerations based on the duration of uniform acceleration for a trapezoidal pulse. The lower curve of figure 11 represents the area of uninjured, undebilitated exposures that have been endured by human volunteers in catapult seat experiments. The top curve shows data for animal exposures to forces that were survivable with moderate injury. The central curve (shaded band) is the assumed safe design limit for ejection seat performance. This band was established from static compressive strength of cadaver vertebrae loaded to fracture point. The conclusion from these tests of the vertebrae was that 20g of 0.005- to 0.5-sec duration can be tolerable. These data are often referenced for aircraft crash studies in crashes where the major forces compress the spine and may cause spinal injuries.

In addition to the Eiband curves, a number of indices (ref. 30) are utilized in assessing human tolerance to various crash loadings. One such index is the dynamic response index, which is a one-degree-of-freedom, damped spring mass model of the upper torso (spine) shown in figure 12. The index is the maximum response acceleration in g units from inputs to the spinal model, which has a natural frequency ω of approximately 52.9 rad/sec and a damping ratio ζ of 0.224, derived from U.S. Air Force experiments (ref. 31).

In figure 13, the dashed line with the symbols represents the percentage probability of spinal injury as a function of DRI based upon in-the-field ejection seat experience (ref. 30). The solid curve represents results from experiments using cadavers. The DRI curve shows reasonably good correlation for the trapezoidal ejection seat pulses, whereas the cadaver results indicate a higher probability of injury than the operational data for a given DRI.

To establish a possible correlation between the normal impulses from the crash data, the Eiband curve, and DRI were determined for various pulse shapes (ramp triangle, symmetric triangle, abrupt leading-edge triangle, trapezoidal, half-sine, and rectangular wave) having a constant amplitude of 20g but a range of pulse durations between 0.005 to 0.48 sec. The results are shown in figure 14 as the ratio of DRI to input plotted as a function of the impulse $\ddot{Z}\,\Delta t$, which produced the responses for the various pulse shapes. For instance, consider the 20g trapezoidal pulse which results in amplification of the input at values of impulse greater than 0.9 and rapidly reaches ratios of essentially 1.5 at an impulse value of approximately 1.5. The triangular pulses, on the other hand, are just beginning to be amplified at the same impulse value of 1.5. For further clarification of pulse shape amplification, see reference 28.

From a different perspective, for the same vertical velocity change as the trapezoidal pulse, the triangular pulses (with approximately the same duration as the trapezoidal pulse) would have a value of $\ddot{Z}\,\Delta t$ approximately twice that of the trapezoidal pulse, but because of less severe amplification (above $\Delta t = 0.07$ sec), the DRI values are comparable in many cases. Since the durations for most of the data analyzed from the tests, representative of severe but potentially survivable crashes, were generally greater than 0.05 sec and triangular in shape, it appears that the use of data based on trapezoidal pulses would not be realistic for evaluating human tolerance in airplane crashes but are more representative of ejection seat performance.

AIRCRAFT SUBFLOOR RESPONSE TO CRASH LOADINGS

Experimental Studies

The development of structural concepts to limit the load transmitted to the occupant has been studied as part of the crash dynamics research conducted at LaRC in determining crash loads and identifying structural failure mechanisms during aircraft crashes. The objective of this research is to attenuate the load transmitted by a structure either by modifying the structural assembly, changing the geometry of its elements, or adding specific load-limiting devices to help dissipate the kinetic energy. Recent efforts in this area at LaRC have concentrated on the development of crashworthy subfloor systems. These subfloor systems provide a high-strength structural floor platform to retain the seats and a crushable zone to absorb energy and limit vertical loads by stroking (ref. 32).

The concept of stroking and available stroke is paramount in determining the load attenuating capabilities of different design approaches in aircraft component design. Shown in figure 15 are three load attenuating zones which exist between an occupant and the impact surface during vertical descent: the landing gear, the fuselage floor structure, and the aircraft seat. Landing-gear stroking during full-scale testing of aircraft was of limited value for energy dissipation although useful in helicopter crash dynamics. For an upward human acceleration tolerance of 25g (ref. 33), a relationship between stroke and vertical descent velocity can be established for a constant stroking device which fully strokes in less than the maximum time allowable (0.10 sec) for human tolerance. This relationship is illustrated in figure 15. For a condition of a constant 25g deceleration stroke, the maximum velocity decrease for the stroking available is 12.2 m/sec (40 fps) for the seats (assuming 30-cm (12-in.) stroke) and 8.2 m/sec (27 fps) for the subfloor (assuming 15-cm (6-in.) stroke). For a combination of stroking seat and stroking subfloor, the maximum velocity decrease becomes 15.2 m/sec (50 fps). These vertical

sink rates are comparable to the U.S. Army Design Guide recommendations for crashworthy seat design (ref. 33).

The importance of providing as much stroking distance as possible is vividly illustrated in figure 16. Figure 16(a) is an overall view of a twin-engine airplane that crashed on August 30, 1978, shortly after takeoff from the North Las Vegas Airport, Nevada, killing all 10 people aboard. An interior view of the airplane after the seats have been removed is shown in figure 16(b). As may be noted in this figure, the floor is very wavy, seat rails are broken, and floor structure is crumpled under the front legs at the seat locations. These conditions are indicative of the high loads transmitted to the seats and occupants through the relatively stiff floor structure. As illustrated in figure 16(c), the intersections of the longitudinal beams and the lateral bulkheads in the floor form "hard points" or columns, which are very efficient load paths from the underbelly of the airplane to the seat rails. Consequently, any crushing of the floor that might occur in a crash situation probably will be at too severe a level for occupant survivability. Thus, the need exists for structural designs which allow for controlled structural collapse to absorb energy and to limit the vertical loads to human tolerance levels over as much distance as possible.

A number of subfloor specimens with various load-limiting concepts were constructed at LaRC and tested statically and dynamically to evaluate their performance (ref. 32). These subfloors, shown in figure 17, were designed to provide a high-strength structural floor platform to retain the seats but with a crushable zone to absorb energy and limit vertical loads. Experimental static load-deflection data and dynamic deceleration response data for the five subfloors indicated that the high-strength floor platform performed well in that structural integrity and residual strength was maintained throughout the loading cycle. The data, shown in figure 18, also indicated that some of the subfloor crush zones were more effective than others in providing nearly constant load (on a lead mass representing an occupant) for a range of displacements. Two of the more promising concepts, that is, notched corners only and the corrugated beams with notched corners, were selected for further evaluation in full-scale crash tests. An airplane equipped with a notched corner subfloor is illustrated in figure 19. The current full-scale crash test assessment of these subfloor concepts shows a significant reduction in cabin decelerations over the unmodified subfloor.

Analytical Studies

A finite-element computer program DYCAST (refs. 34 and 35) was used in a simplified and economical manner to model the complex nonlinear response of the aircraft subfloor sections to crash loads. Figure 20 illustrates the finite-element idealization used in applying the DYCAST computer program to the subfloor having a corrugated beam with notched corners. Only half the structure is modeled to take advantage of symmetry of the structure. The seat tracks and stiffeners of the floor platform are modeled as beam elements; the floor skin, as triangular membrane elements; and the structure beneath the floor platform, by five nonlinear springs at the floor beam-frame intersections. Static load-deflection data were used to characterize the nonlinear crush zone of the subfloor. The capability of DYCAST to accurately analyze the load-limiting subfloors was verified by comparisons between experimental and analytical response data of a rigid lead mass representing an occupant. Good correlation was indicated between the predicted deceleration magnitude and duration and the lead mass (occupant) experimental responses for the subfloors in which the static deformation mode closely approximated the dynamic deformation behavior as is shown in

figure 21 for the corrugated beam with notched corner subfloor. For other subfloor configurations, as shown in figure 22, the comparisons were good only for the initial peak deceleration and limited subsequent response where the static and dynamic deformation modes corresponded.

The analysis and correlation with experimental results have shown the usefulness of statically determined crush data for dynamic analysis; however, the results also indicate that the analyst must exercise care and have some assurance that the static deformation behavior will approximate the dynamic deformation behavior.

SEAT RESPONSE TO CRASH LOADINGS

Experimental Studies

In load-limiting seat design, the concepts of available stroke are paramount in determining the load attenuating capabilities of different design configurations. Consider an idealized man/seat model consisting of a two-mass system connected by nonlinear springs with viscous damping as follows:

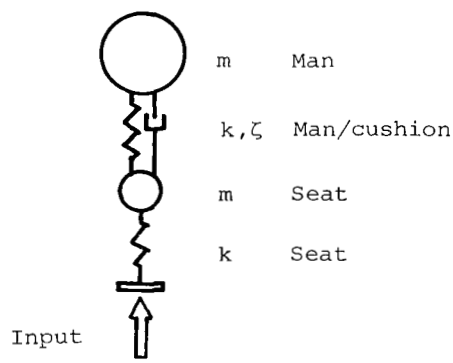

The occupant response to a specific input at the seat base can be amplified, as illustrated in the following sketch, if the stiffness of the seat and associated fundamental frequencies are of the same order as the input forcing frequency:

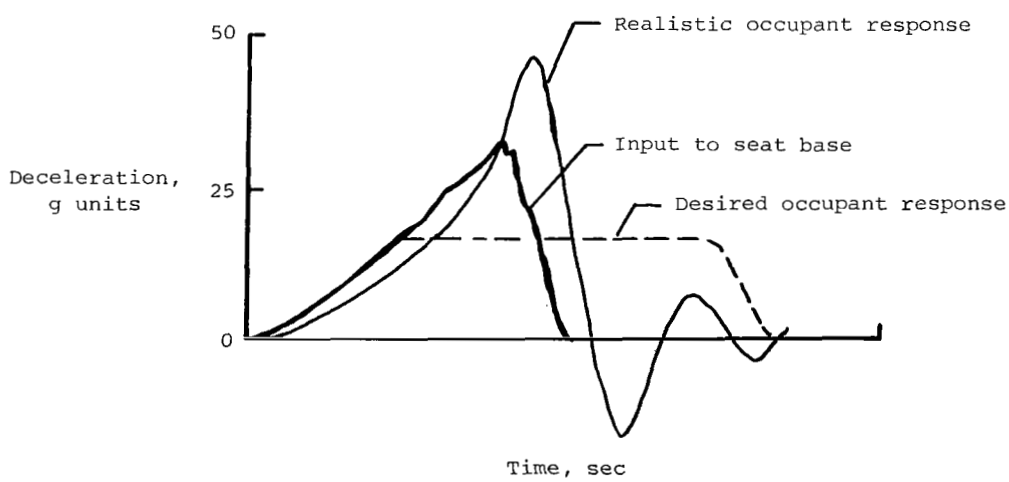

This undesirable amplification was observed experimentally when testing seats dynamically, as in tests conducted at CAMI (FAA Civil AeroMedical Institute), by using a test sled. (See ref. 36.) With this dynamic seat test sled, different seat configurations were studied to determine their response characteristics. The seats and restraint systems were dynamically loaded by 50th percentile, Hybrid II, anthropomorphic dummies instrumented with accelerometers.

Time histories of dummy pelvis accelerations were recorded during two different impact loadings as shown in figure 23 with the dummy installed in a standard seat and in a ceiling-suspended, load-limiting seat. For the "vertical" impulse (fig. 23(a)), the seats and dummy were positioned to impact at a pitch angle (angle between dummy spine and direction of sled travel) of -30° and a roll angle of 10°. In the "longitudinal" pulse (fig. 23(b)), the seats were yawed 30° to the direction of sled travel. The sled pulses are also included in the figure and represent the axial impulse imparted to the inclined dummies. The X- and Z-axes of the dummy are local axes perpendicular and parallel to its spine, respectively. The figure shows that for both impact conditions the load-limiting seat generally provided a sizable reduction in pelvis acceleration over those recorded during similar impacts using the standard seat. In contrast, the standard seat exhibits amplified acceleration levels over those input to the sled as it decelerated.

Load dissipating seats with proper restraints can be designed to provide a measure of load reduction by stroking. Vertical stroking of general aviation seats is more critical than horizontal stroking from the allowable human tolerance standpoint and deserves considerable attention since little crushable structure in the vertical direction is available in most subfloor structures of single-engine general aviation airplanes. The concept of vertical-stroking, floor-supported passenger seat is shown in figure 24. The energy absorbing seat is composed of two four-bar linkages in parallel. The floor is the fixed bar, the seat pan the top bar, and the front and rear legs the other two bars. A load limiter was attached on each side diagonally between the seat pan rear leg joint and the floor front leg joint. The load limiter, shown in figure 25, absorbed energy by bending a wire over rollers in a trolley. The trolley is attached to a pin between the rear leg and the seat pan. During seat stroking, the trolley forced the wire loop along the wire. The static load-deflection curve for the load limiter is shown in figure 26 for two specific tests. Vertical drop tests of this vertical-stroking, load-limiting seat were performed in a test apparatus shown in figure 27. The test apparatus consists of a large cylindrical section with wedges attached to the test apparatus to shape the "crash" pulse upon impact into a bed of glass beads. The cylinder can be rotated relative to the wedges to vary the vector inputs. The floor inside the cylinder consisted of an aluminum plate mounted on a thick plywood board. The plywood was used to isolate the test specimens from the high-frequency ringing of the test vehicle. The load-limiting seat was mounted on the aluminum plate. A 50th-percentile, Hybrid II, anthropomorphic dummy was used throughout the tests and was restrained to the seat with a four-point restraint shoulder harness and lap belt. The test results from a vertical drop test at 0° pitch attitude are shown in figure 27. (See ref. 36.)

The raw vertical floor acceleration data and the filtered 20-Hz data are shown in the top plot of the figure. The filtered floor acceleration data peaked at 37g with a pulse duration of 0.07 sec. This vertical acceleration pulse closely approximates the normal pulse obtained from NASA crash test 18 (table I). The filtered vertical acceleration measured at the seat pan reached 15g, as shown in the second plot, and the acceleration remained constant for about 0.04 sec, then peaked at 17g before diminishing to 0g. The total pulse duration was 0.10 sec. The load-limiting

seat was demonstrably effective in attenuating the vertical pulse transmitted to the seat to a human-tolerable value.

The seat pulse superimposed on the floor pulse is shown in the third plot. The relative magnitude and duration of the pulses can readily be seen. The pelvis acceleration data were lost and the chest data were analyzed instead. The normal chest acceleration was filtered at 180 Hz and is shown in the last plot. An average acceleration of 15g with a pulse duration of 0.094 sec was obtained. A 35g spike is shown in the acceleration trace. The spike is more noticeable when compared with the smooth traces of the floor and seat pulses because it was filtered at 180 Hz, whereas the floor and seat accelerations were filtered at 20 Hz. The spike has an equivalent frequency of 50 Hz and would have been considerably attenuated by filtering at 20 Hz.

Analytical Studies

Analytical efforts have been directed toward developing a good mathematical model that will aid in designing load-limiting seats. In earlier studies, computer program MSOMLA (Modified Seat Occupant Model for Light Aircraft) was used to simulate the occupant response to a full-scale crash by using a simplified one-dimensional nonlinear spring for the seat (ref. 36). However, when a more sophisticated seat model was needed to model the floor-mounted load-limiting seat, the DYCAST computer code (refs. 34 and 35) was chosen. The seat-occupant model used for the analysis of the 0° pitch, 12.8 m/sec vertical drop test is shown in figure 28. The model is of necessity a hybrid model consisting of finite elements and nonlinear springs with the spring characteristics specified in tabular form. In this model, the wire bending load limiter, shoulder harness, lap belt, seat back stiffness, and pelvis stiffness are modeled as nonlinear springs. The occupant consists of three masses connected by pin jointed beams. The motion of the pelvis mass is followed by node 3 of the pelvis spring, which is restricted by multipoint constraints to move along the seat pan. The seat is modeled by using beams with the seat mass distributed at the nodes. The seat and occupant are given an initial vertical velocity of 12.8 m/sec. The experimental deceleration pulse was input by applying a time-dependent stopping force to node 1, which represents the mass of the test vehicle. The stopping force corresponded to the triangular deceleration pulse shown with a peak deceleration of 36.5g, the pulse starting at time 0.02 sec with a duration of 0.076 sec, which corresponds to a typical vertical cabin pulse in a severe but potentially survivable general aviation crash. (See table I.)

DYCAST was used with the Newmark Beta time integration technique with an average time step of 1×10^{-4} sec. The problem executed in about 14 min on a CDC® CYBER 175 computer system to simulate 0.10 sec of real time. The comparison of the DYCAST model data with the 0° pitch experimental vertical drop test data for the seat pan and chest accelerations is shown in figure 29. With the exception of the initial vertical chest deceleration spike, the comparison shows overall good agreement between the model and the experimental data. At the top of figure 29 are three computer graphics drawings of the seat and occupant positions at times 0, 0.05, and 0.10 sec. From the plot of the seat position at time 0.05 sec, it is apparent that for the 0° pitch vertical drop, the seat back spring is compressed as the seat moves forward. At this time, the lap belt and shoulder harness become slack. Experimentally, the dummy rebounded and loaded the belts at time 0.14 sec.

Comparison of DYCAST predictions and experimental measurements of peak accelerations and seat stroking are given in table II. The wire bending energy absorber stroke was measured to be 17.5 cm (6.9 in.), whereas DYCAST slightly underpredicts

at 16.5 cm (6.5 in.). Total available wire bending stroke is approximately 29 cm (11.5 in.). Forward and vertical seat stroke also compared quite well with the experimentally measured values.

In summary, the DYCAST computer model has proven to be very useful for detailed modeling of load-limiting seats with a hybrid finite-element approach. Since the model is general, the developer is free to start with a simple seat and occupant and to increase the sophistication as needed for the task at hand. Further development of the occupant with torsional springs, a more realistic spine, and even multiple seats and occupants is being contemplated.

EMERGENCY LOCATOR TRANSMITTER TESTS

A side issue, and an interesting one, has resulted from the work on crash dynamics reported to this point; that issue is a study of problems associated with the emergency locator transmitter. General aviation airplanes have, since the 1970's, been required to carry an ELT to expedite the location of crashed airplane by automatically activating and transmitting a distress signal in the event of a crash. However, a high rate of nondistress activation and failures to activate in a crash situation have severely limited the usefulness of these potentially life-saving devices. Suspected sources of the problem, according to a recent NTSB review (ref. 37), are improper mounting and/or mounting location in the airplane, short circuits, vibration sensitivity, battery failures, and antenna location. LaRC has assisted the FAA and industry through Radio Technical Commission for Aeronautics (RTCA) Special Committee 136 to study in depth the ELT problems and to seek solutions. (See refs. 38 and 39.)

LaRC demonstrated ELT sensor activation problems by mounting a sampling of ELT specimens in full-scale crash test airplanes and in the test apparatus used for dynamic seat testing, which is fully described in a previous section. The test apparatus is shown in figure 30 with an actual airplane tail section mounted in its interior. The ELT as mounted in the tail section represents a typical mounting location in general aviation airplanes. Decelerations at the base of the airplane section, responses of the bulkheads and webs, and the response of the ELT are recorded along with activation or no activation signals.

The test apparatus permits an extension of test data on ELT's acquired during crash tests of full-size airplanes at the Langley Impact Dynamics Research Facility. For example, the data in figure 31 are a comparison of the longitudinal deceleration on an ELT in a full-scale crash test with a simulated crash pulse in the test rig. As indicated in the figure, both the characteristic shape of the faired crash pulse and structural resonances are reproduced by the test apparatus (ref. 40).

Evaluation of test results has indicated that one of the ELT performance problems is the vibration sensitivity of the ELT inertia switches or sensors shown at the top right of figure 32. In the figure, the ratio of response to input for a commercial sensor is plotted against frequency. Data indicate that the resonant frequencies of most commercial sensors fall well into the range of frequencies of local structural vibrations that exist on light airplanes. On the other hand, the frequency range of crash pulses which need to be detected is on the lower end of the frequency spectrum. Thus, the sensors are often too responsive to the local structural vibrations. This undesirable sensitivity can cause unwarranted activations in some cases or may prevent the sensor from activating the ELT in a crash situation because the on-off-on-off response can prevent the sensor from activating.

A suggested improvement for a sensor is also shown in figure 32. By designing the sensor to have a much lower resonant frequency, the switch can still detect the low-frequency crash pulse but will attenuate the higher frequencies of vibration because of the inherent behavior of the response of the sensor. An experimental sensor with a lower resonance has been tested and found to possess the desirable properties as illustrated in the figure by the dashed line.

CONCLUDING REMARKS

Results of the testing, observations, assessments, and findings presented herein indicate that crash dynamics is becoming a workable discipline. This is not to imply that research in crash dynamics, or specifically in general aviation crash dynamics, has been completed. It does indicate that enough data have been gathered and enough successful simplified analyses have been conducted to encourage thinking of crash dynamics design as an emerging, workable discipline. The approach of using selective testing coupled with supportive analysis to assess preliminary design concepts of crash dynamics is feasible and, with practice, can become a workable design methodology. Specific comments relative to the general aviation crash dynamics research surveyed in this paper are as follows:

1. Full-scale aircraft testing has produced identifiable representative floor pulses. These floor pulses can be related to the flight parameters at impact with uncoupled, simple impulse-momentum relationships which lend themselves to such applications, as postcrash analysis and comparisons with human tolerance data.

2. Load-limiting subfloor concepts were developed that feature a strong upper floor configuration to resist overturning seat moments and a crushable subfloor that distributes the loads evenly across the fuselage. Static crush tests of simplified components that characterize the nonlinear load-deflection behavior of the crushable elements of the subfloor are used in mathematical models to predict dynamic behavior. The static tests should produce collapse mechanisms similar to those expected dynamically.

3. Load-limiting seat concepts were developed that help reduce the loads transmitted from the airframe to the occupant. The multiple-degree-of-freedom seat/occupant/restraint systems can produce dynamic amplification factors that significantly increase occupant-experienced loads if the seats are relatively stiff with high fundamental frequencies. Computer simulations of load-limiting seats capitalize on knowing the static crush characteristics of the component seat structure to help predict mathematically the dynamic behavior of the seat/occupant/restraint system response.

4. Data from crash tests at the Langley Research Center indicate that the longitudinal crash environment imposed on emergency locator transmitters (ELT's) in crash situations is basically a low-frequency loading pulse; however, high amplitude, higher frequency local structural resonances are superimposed on the crash pulse. Impact sensors typical of those used in ELT's were found to be too sensitive to the structural vibrations. A low-frequency switch design was found to have desirable response characteristics in that it is sensitive to low-frequency crash pulses and is less sensitive to higher frequencies in the range of local structural vibrations.

5. The methods and concepts developed in the general aviation crash dynamics program are being examined and evaluated to determine their applicability to a current transport crash dynamics program. The transport program facilitates the inte-

gration of crashworthy structural design concepts into transport design methods and considers airframe, seat, floor, fuel tanks, and landing-gear behavior. The research efforts in the general aviation program are expected to make possible future airplane design concepts having enhanced survivability under specified crash conditions with little or no increase in weight and having acceptable costs.

Langley Research Center
National Aeronautics and Space Administration
Hampton, VA 23665
March 16, 1984

REFERENCES

1. De Haven, Hugh: Causes of Injury in Lightplane Accidents. Aero Digest, vol. 44, no. 5, Mar. 1, 1944, pp. 51-55, 206.

2. Hasbrook, A. Howard: What a Spray Plane Should Have. Aviat. Week, vol. 52, no. 7, Feb. 13, 1950, pp. 25-27, 30-31.

3. Hoekstra, Harold D.; and Huang, Shung-Cha: Safety in General Aviation. Flight Safety Foundation, Inc., 1971.

4. Pinkel, I. Irving; Preston, G. Merritt; and Pesman, Gerald J.: Mechanism of Start and Development of Aircraft Crash Fires. NACA Rep. 1133, 1953. (Supersedes NACA RM E52F06.)

5. Reed, W. H.; Robertson, S. H.; Weinberg, L. W. T.; and Tyndall, L. H.: Full-Scale Dynamic Crash Test of a Douglas DC-7 Aircraft. FAA-ADS-37, Apr. 1965.

6. Bigham, James P., Jr.; and Bingham, William W.: Theoretical Determination of Crash Loads for a Lockheed 1649 Aircraft in a Crash Test Program. Tech. Rep. ADS-15, FAA, July 1964.

7. Turnbow, J. W.; Carroll, D. F.; Haley, J. L., Jr.; and Robertson, S. H.: Crash Survival Design Guide. USAAVLABS Tech. Rep. 70-22, U.S. Army, Rev. Aug. 1969. (Available from DTIC as AD 695 648.)

8. Army Aviation Safety - Crash Injury and Crashworthiness Programs. TREC Tech. Rep. 60-77, U.S. Army, Dec. 30, 1960.

9. Foulk, James B.: Survivability of the Army/Sikorsky YUH-60A Helicopter. Preprint No. 1011, 32nd Annual National Forum, American Helicopter Soc., May 1976.

10. Carnell, Brian L.: Crashworthiness Design Features for Advanced Utility Helicopters. Aircraft Crashworthiness, Kenneth Saczalski, George T. Singley III, Walter D. Pilkey, and Ronald L. Huston, eds., Univ. Press of Virginia, c.1975, pp. 51-63.

11. Mazza, L. Thomas; and Foye, R. L.: Advanced Composite Airplane Program - Preliminary Design Phase. Preprint No. 80-45, 36th Annual National Forum Proceedings, American Helicopter Soc., May 1980.

12. Thomson, Robert G.; and Goetz, Robert C.: NASA/FAA General Aivation Crash Program - A Status Report. J. Aircr., vol. 17, no. 8, Aug. 1980, pp. 584-590.

13. Eiband, A. Martin; Simpkinson, Scott H.; and Black, Dugald O.: Accelerations and Passenger Harness Loads Measured in Full-Scale Light-Airplane Crashes. NACA TN 2991, 1953.

14. Reed, William H.; and Avery, James P.: Principles for Improving Structural Crashworthiness for STOL and CTOL Aircraft. USAAVLABS Tech. Rep. 66-39, U.S. Army, June 1966. (Available from DTIC as AD 637 133.)

15. Vaughan, Victor L., Jr.; and Alfaro-Bou, Emilio: Impact Dynamics Research Facility for Full-Scale Aircraft Crash Testing. NASA TN D-8179, 1976.

16. Alfaro-Bou, Emilio; and Vaughan, Victor L., Jr.: Light Airplane Crash Tests at Impact Velocities of 13 and 27 m/sec. NASA TP-1042, 1977.

17. Castle, Claude B.; and Alfaro-Bou, Emilio: Light Airplane Crash Tests at Three Flight-Path Angles. NASA TP-1210, 1978.

18. Castle, Claude B.; and Alfaro-Bou, Emilio: Light Airplane Crash Tests at Three Roll Angles. NASA TP-1477, 1979.

19. Vaughan, Victor L., Jr.; and Alfaro-Bou, Emilio: Light Airplane Crash Tests at Three Pitch Angles. NASA TP-1481, 1979.

20. Vaughan, Victor L., Jr.; and Hayduk, Robert J.: Crash Tests of Four Identical High-Wing Single-Engine Airplanes. NASA TP-1699, 1980.

21. Williams, M. Susan; and Fasanella, Edwin L.: Crash Tests of Four Low-Wing Twin-Engine Airplanes With Truss-Reinforced Fuselage Structure. NASA TP-2070, 1982.

22. Alfaro-Bou, Emilio; Williams, M. Susan; and Fasanella, Edwin L.: Determination of Crash Test Pulses and Their Application to Aircraft Seat Analysis. SAE Tech. Paper 810611, Apr. 1981.

23. Preston, G. Merritt; and Pesman, Gerard J.: Accelerations in Transport-Airplane Crashes. NACA TN 4158, 1958.

24. Reed, W. H.; Robertson, S. H.; Weinberg, L. W. T.; and Tyndall, L. H.: Full-Scale Dynamic Crash Test of a Lockheed Constallation Model 1649 Aircraft. FAA-ADS-38, Oct. 1965.

25. Acker, Loren W.; Black, Dugald O.; and Moser, Jacob C.: Acceleration in Fighter-Airplane Crashes. NACA RM E57G11, 1957.

26. Carden, Huey D.: Correlation and Assessment of Structural Airplane Crash Data With Flight Parameters at Impact. NASA TP-2083, 1982.

27. Safety Report: General Aviation Crashworthiness Project, Phase One. NTSB/SR-83/01, National Transportation Safety Board, June 27, 1983. (Available from NTIS as PB83-917004.)

28. Carden, Huey D.: Impulse Analysis of Airplane Crash Data With Consideration Given to Human Tolerance. SAE Tech. Paper Ser. 830748, Apr. 1983.

29. Eiband, A. Martin: Human Tolerance to Rapidly Applied Accelerations: A Summary of the Literature. NASA MEMO 5-19-59E, 1959.

30. Desjardins, S. P.; Laananen, D. H.; and Singley, G. T., III: Aircraft Crash Survival Design Guide. Volume I - Design Criteria and Checklists. USARTL-TR-79-22A, U.S. Army, Dec. 1980. (Available from DTIC as AD A093 784.)

31. Payne, Peter R.; and Stech, Ernest L.: Dynamic Models of the Human Body. AMRL-TR-66-157, U.S. Air Force, Nov. 1969. (Available from DTIC as AD 701 383 and also available as NASA TM X-67038.)

32. Carden, Huey D.; and Hayduk, Robert J.: Aircraft Subfloor Response to Crash Loadings. SAE Tech. Paper Ser. 810614, Apr. 1981.

33. Dynamic Sci. Eng. Operations: Crash Survival Design Guide. USAAMRDL Tech. Rep. 71-22, U.S. Army, Rev. Oct. 1971. (Available from DTIC as AD 733 358.)

34. Pifko, A.; Levine, H. S.; and Armen, H., Jr.: PLANS - A Finite Element Program for Nonlinear Analysis of Structures. Volume I - Theoretical Manual. NASA CR-2568, 1975.

35. Pifko, A.; Armen, H., Jr.; Levy, A.; and Levine, H.: PLANS - A Finite Element Program for Nonlinear Analysis of Structures. Volume II - Users' Manual. NASA CR-145244, 1977.

36. Fasanella, Edwin L.; and Alfaro-Bou, Emilio: NASA General Aviation Crashworthiness Seat Development. [Preprint] 790591, Soc. Automot. Eng., Apr. 1979.

37. Special study - Emergency Locator Transmitters: An Overview. Rep. No. NTSB-AAS-78-1, Jan. 26, 1978.

38. RTCA SC-136: Emergency Locator Transmitter (ELT) Equipment Installation and Performance. DO-182, Radio Tech. Comm. Aeronaut., Nov. 17, 1982.

39. RTCA SC-36: Minimum Operational Performance Standards for Emergency Locator Transmitters. DO-183, Radio Tech. Comm. Aeronaut., May 13, 1983. (Supersedes RTCA/DO-145, RTCA/DO-146, and RTCA/DO-168.)

40. Carden, Huey D.: Evaluation of Emergency-Locator-Transmitter Performance in Real and Simulated Crash Tests. NASA TM-81960, 1981.

TABLE I.- SUMMARY OF DATA FROM CONTROLLED CRASH TESTS OF AIRPLANES

(a) Experimental and calculated normal pulse parameters

Test	Flight-path angle, γ, deg	Pitch angle, θ, deg	Flight-path velocity, V_{fp}, m/sec	Experimental normal pulse parameters				Calculated normal pulse parameters	
				Maximum deceleration, $\ddot{z}_{a,max}$, g units	Pulse duration, Δt, sec	Velocity change, ΔV_Z, m/sec	Impulse, $\ddot{z}_{a,max}\ \Delta t$, sec	Impulse, $\ddot{z}_{a,max}\ \Delta t$, sec	Velocity change, ΔV_Z, m/sec
2(ref. 26)	-16	-12	27	20	0.089	8.5	1.78	1.49	7.44
3	-18.75	-18	26.2	28	.05	8.74	1.40	1.63	8.42
4	-15	4	27	16	.102	8.5	1.63	1.42	6.99
5	-20.5	-19.5	26.1					1.76	9.14
6	-16	14	27	18	.110	10.4	1.98	1.47	7.44
7	-47.5	-47.25	28.6	20	0.174	20.73	3.48	2.92	21.1
8	-30	-31	27	18	.135	13	2.43	2.36	13.5
9	-16	-13	26.3					1.44	7.25
10	-18	-14	27.8					1.70	8.59
11	-31	-27	25	12	.132	10	1.58	2.34	12.87
12	-15	9	25	12	0.149	9.5	1.79	1.30	6.47
13	-29	-26	25	27	.049	13	1.32	2.22	12.12
14	-16.75	-11.75	32.7					1.88	9.42
15	-18	-12	41	46	.064	17	2.94	2.53	12.67
16	-15	-4	40	46	.054	15	2.48	2.11	10.35
17	-30	-38	40	42	0.097	19	4.07	3.22	20.0
18	-30	-31	27.9	27.2	.083	11.3	2.26	2.34	13.5
19	-15	-17.7	27	16	.12	10.6	1.92	1.38	6.99
20	-15.4	2	26.6	31	.057	9.1	1.77	1.43	6.99
21	-30	-29.5	27.1	29.9	.096	12.3	2.87	2.39	13.5
FAA-1	-32	-30	25	21	0.120	11	2.52	2.34	13.24
FAA-2	-17	-13.5	23	7	.160	6	1.12	1.33	6.72
FAA-3	-34.5	-39	25.9	18	.12	13.8	2.2	2.33	14.7
FAA-4	-32	-34.5	25.3	18	.13	14.8	2.34	2.25	13.41
				(a) (b)	(a) (b)	(a) (b)	(a) (b)		
Fighter (ref. 25)	-18	-18	50					3.0	15.45
	-22	-22	50	30	0.142	23	4.26	3.54	18.73
	-27	-27	50	37.5 22	.13 0.21	21.6 22	4.88 4.62	4.13	22.7
Transport (ref. 23)	-14	-14	48.7	11.4	0.25	12	2.85	2.33	11.8
	-27	-27	48.7	23.3	.21	21	4.89	4.02	22.1
Transport (ref. 24) F.S. 1165 F.S. 685 c.g.	-6	-6	57.7	7	0.26	9.4	1.82	1.22	6
Cub type (ref. 13)	-55	-55	26.8						
	-55	-55	21						
	-55	-55	18.8						

[a] Values in the cockpit.
[b] Values at the c.g.

TABLE I.- Concluded

(b) Experimental longitudinal pulse parameters

Test	Flight-path angle, γ, deg	Pitch angle, θ, deg	Experimental longitudinal pulse parameters: Flight-path velocity, V_{fp}, m/sec	Maximum deceleration, $\ddot{x}_{a,max}$, g units	Pulse duration, Δt, sec	Velocity change, ΔV_1, m/sec	Impulse $\ddot{x}_{a,max}\,\Delta t$, sec
2 (ref. 26)	-16	-12	27	19	0.06	6	1.14
3	-18.75	-18	26.2	18	.044	4.3	.79
4	-15	4	27	7	.101	5	.71
5	-20.5	-19.5	26.1				
6	-16	14	27	8	.110	3.1	.86
7	-47.5	-47.25	28.6	8.8	0.144	[a]4.6; 6.8; 9	1.27
8	-30	-31	27	16	.110	6	1.76
9	-16	-13	26.3				
10	-18	-14	27.8				
11	-31	-27	25	28	.138	17.7	3.86
12	-15	9	25	4	0.060	1.2	0.24
13	-29	-26	25	11	.093	5	1.02
14	-16.75	-11.75	32.7				
15	-18	-12	41	16	.058	5	.93
16	-15	-4	40	12	.062	4	.744
17	-30	-38	40	22	0.068	10	1.5
18	-30	-31	27.9	15.2	.090	8.2	1.37
19	-15	-17.7	27	5.5	.088	4	.48
20	-15.4	2	26.6	6.4	.052	1.9	.333
21	-30	-29.5	27.1	14	.112	10.5	1.57
FAA-1	-32	-30	25	22	0.110	8	2.42
FAA-2	-17	-13.5	23	3.5	.060	1.5	.21
FAA-3	-34.5	-39	25.9	17	.13	12	2.21
FAA-4	-32	-34.5	25.3	45	.10	21.5	4.5

Test	γ, deg	θ, deg	V_{fp}, m/sec	$\ddot{x}_{a,max}$, g units (b)	$\ddot{x}_{a,max}$, g units (c)	Δt, sec (b)	Δt, sec (c)	ΔV_1, m/sec (b)	ΔV_1, m/sec (c)	$\ddot{x}_{a,max}\,\Delta t$, sec (b)	$\ddot{x}_{a,max}\,\Delta t$, sec (c)
Fighter (ref. 25)	-18	-18	50	23	16.8	0.10	0.23	12	19.5	2.3	3.81
	-22	-22	50	25	23.3	.18	.21	22	24	4.5	4.92
	-27	-27	50	40	50	.13	.22	26	45	5.2	11.1
Transport (ref. 23)	-14	-14	48.7	7.1		0.21		7.6		1.5	
	-27	-27	48.7	19.2		.36		29.3		6.9	
Transport (ref. 24)	-6	-6	57.7								
F.S. 1165				8		0.235		9.5		1.88	
F.S. 923				8.4		.23		9.5		1.93	
F.S. 685 c.g.				9.0		.23		9.5		2.07	
F.S. 460				9.6		.24		9.5		2.3	
F.S. 195				11.4		.14		9.5		1.6	
Cub type (ref. 13)	-55	-55	26.8	25.2		0.19		27		4.92	
	-55	-55	21	22		.224		21		4.93	
	-55	-55	18.8	18.4		.24		18.8		4.42	

[a]The value 4.6 indicates slide-out (see eq. (21)); 6.8 denotes the average of film and slide-out analysis; and 9 is taken from film analysis.

[b]Values in the cockpit.

[c]Values at the c.g.

TABLE II.- FLOOR-MOUNTED LOAD-LIMITING SEAT COMPARISONS OF EXPERIMENTAL AND ANALYTICAL RESULTS

Impact parameters:

Vertical velocity, m/sec (ft/sec)	12.8 (42)
g_{max}	36.5
Δt, sec	0.076
Pitch, deg	0

	Vertical drop test	DYCAST model
E/A stroke, cm (in.)	17.5 (6.9)	16.5 (6.5)
Forward seat stroke, cm (in.)	13.5 (5.3)	12.7 (5.0)
Vertical seat stroke, cm (in.)	14.5 (5.7)	13.2 (5.2)
Accelerations, body axes, g units, for -		
Chest, forward (after spike)	20	16
Chest, vertical (after spike)	18	20
Seat pan, forward	21	19
Seat pan, vertical	17	22

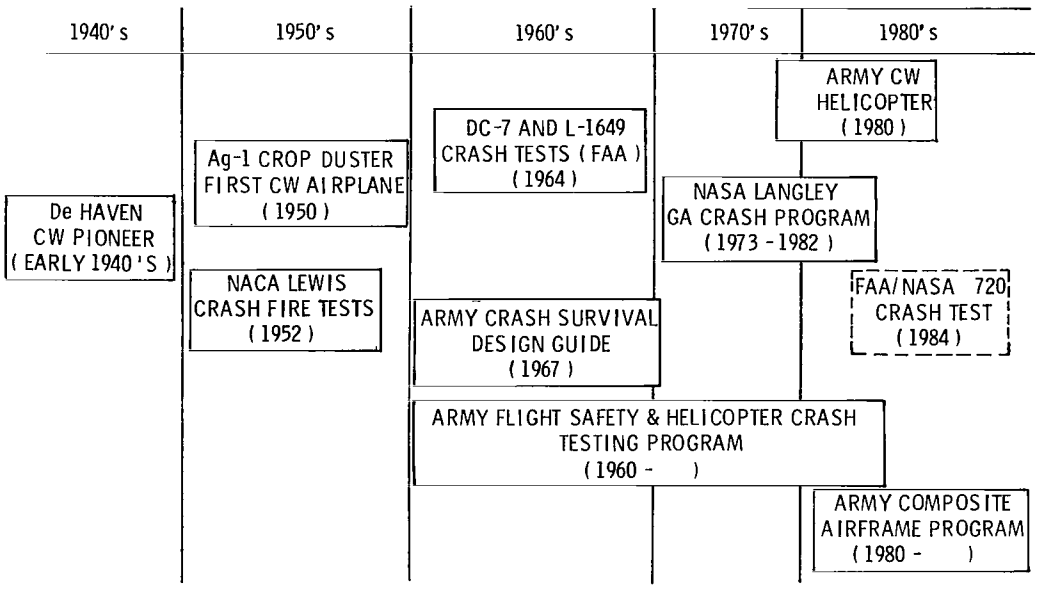

Figure 1.- History of aircraft crash dynamics research.

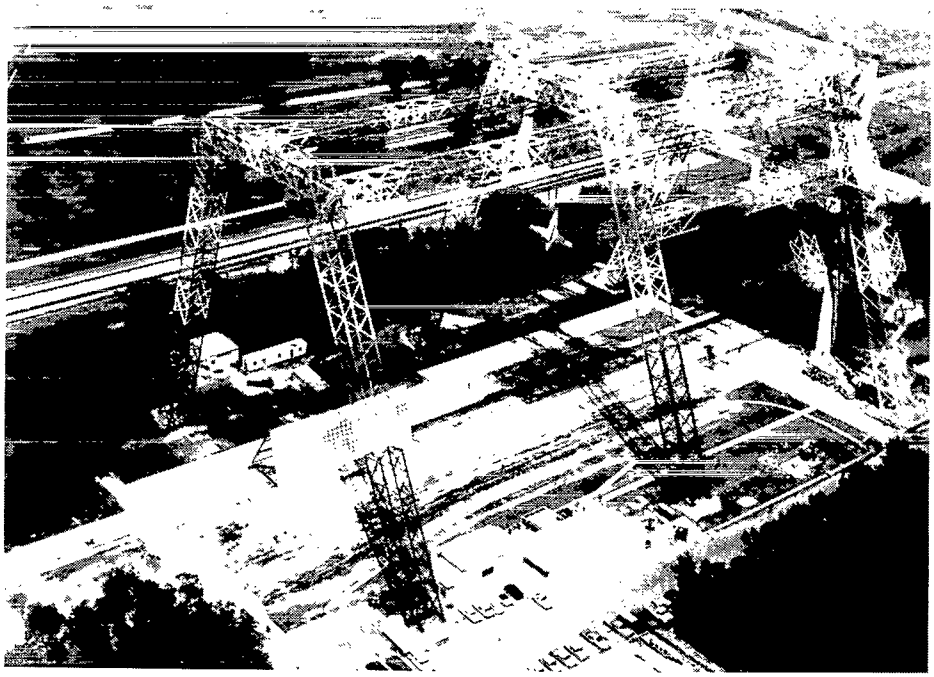

L-74-2505

Figure 2.- Langley Impact Dynamics Research Facility.

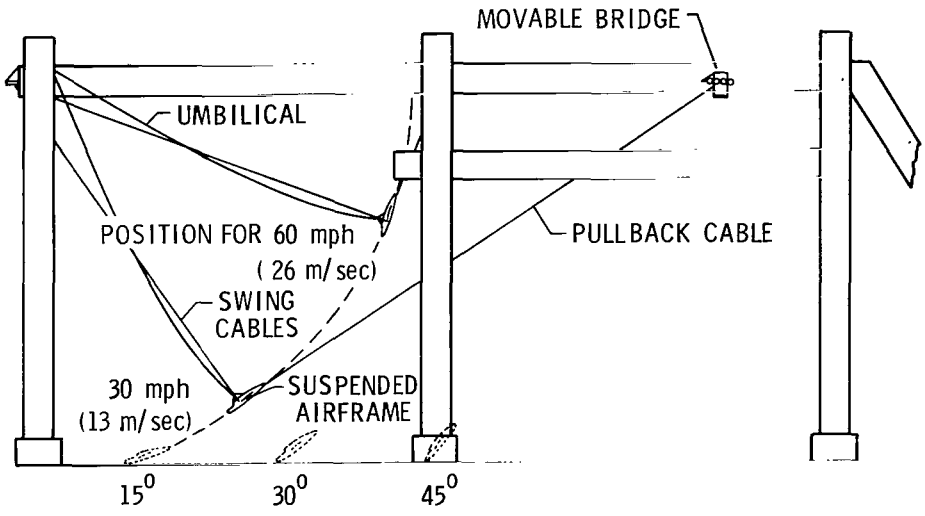

Figure 3.- Full-scale crash test method.

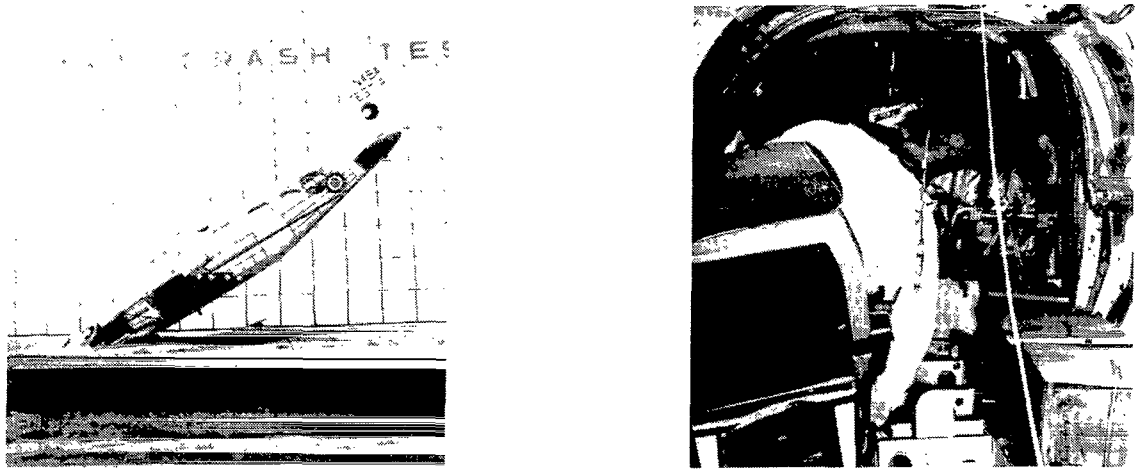

Exterior view at impact

Interior view - postcrash

L-84-29

Figure 4.- Typical general aviation crash test.

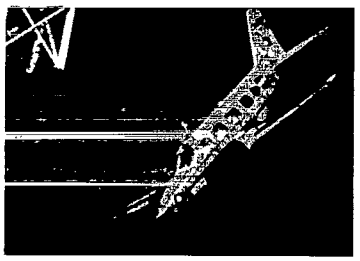

(a) Prior to impact.

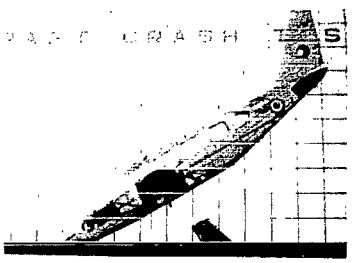

(b) Time = -0.01 sec.

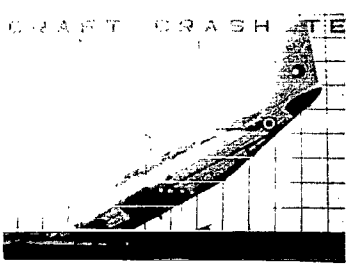

(c) Time = 0.04 sec.

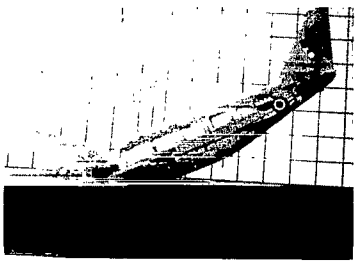

(d) Time = 0.09 sec.

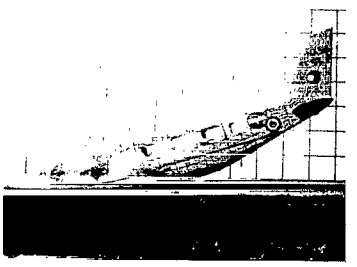

(e) Time = 0.14 sec.

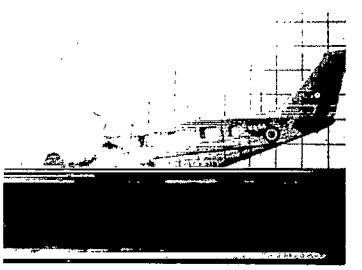

(f) Time = 0.19 sec.

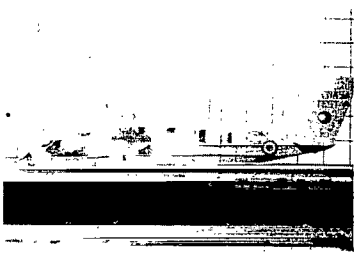

(g) Time = 0.24 sec.

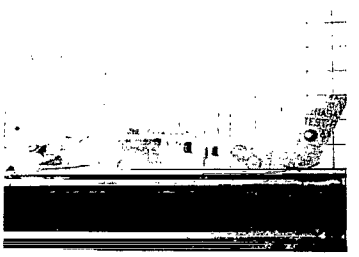

(h) Time = 0.29 sec.

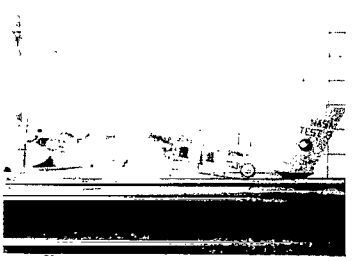

(i) Time = 0.34 sec.

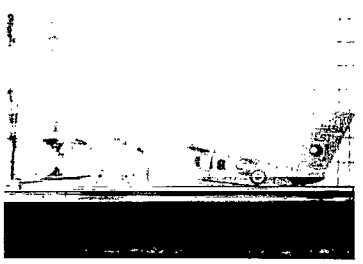

(j) Time = 0.39 sec.

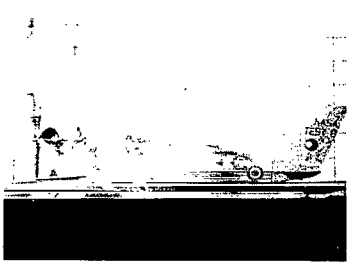

(k) Time = 0.44 sec.

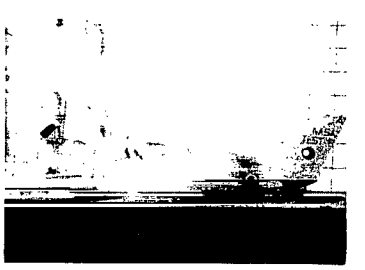

(l) Time = 0.49 sec.

L-75-8921

Figure 5.- Photographic sequence of typical general aviation crash test.

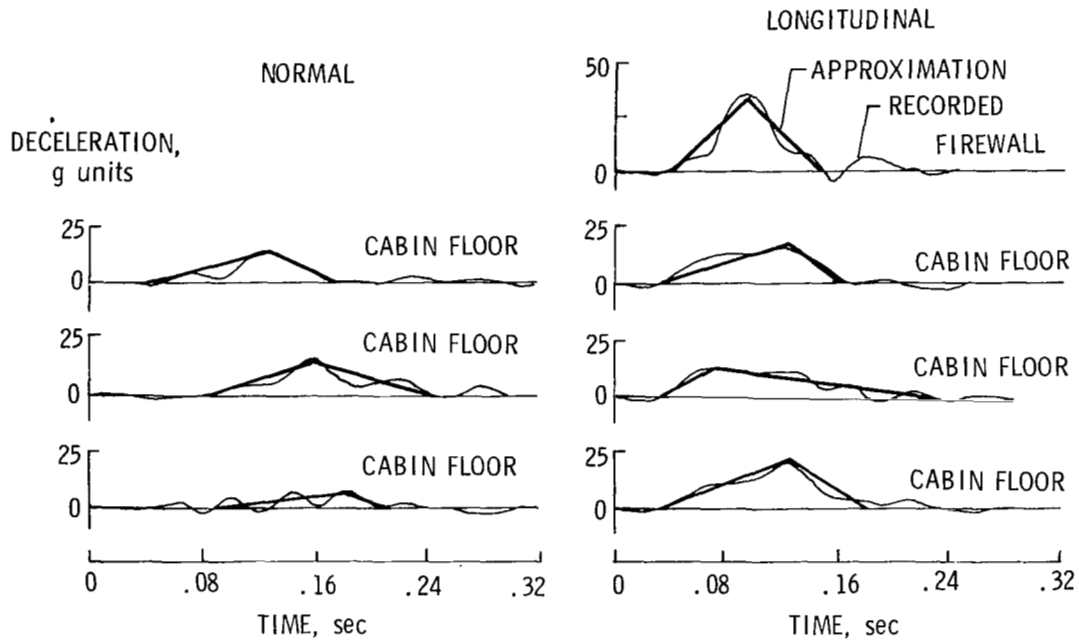

Figure 6.- Typical time histories of normal and longitudinal decelerations of a general aviation aircraft.

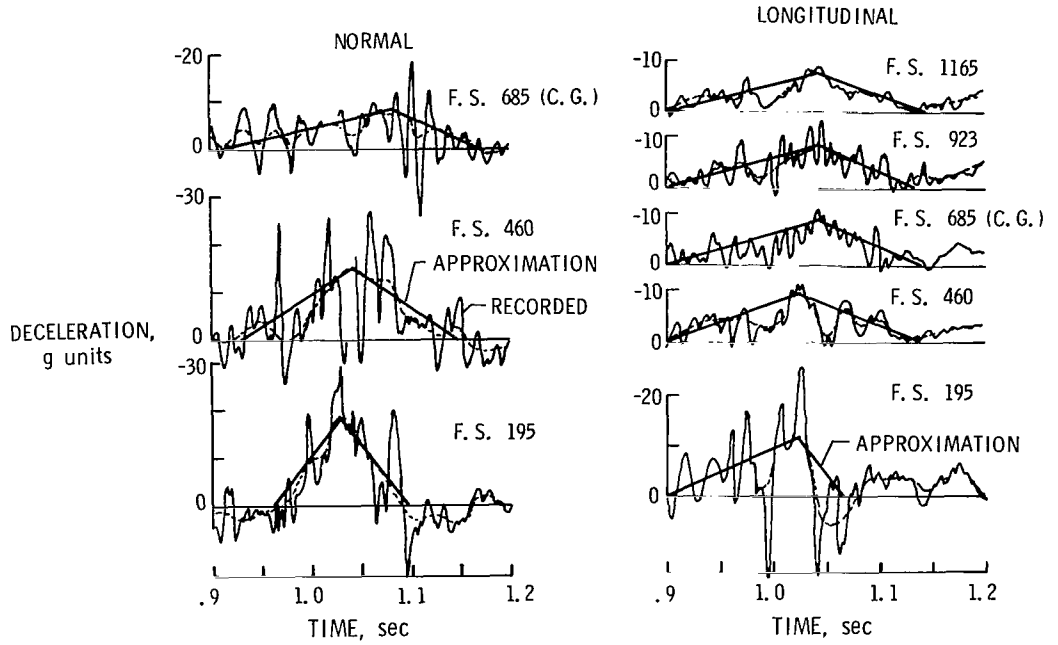

(a) Transport airplane.

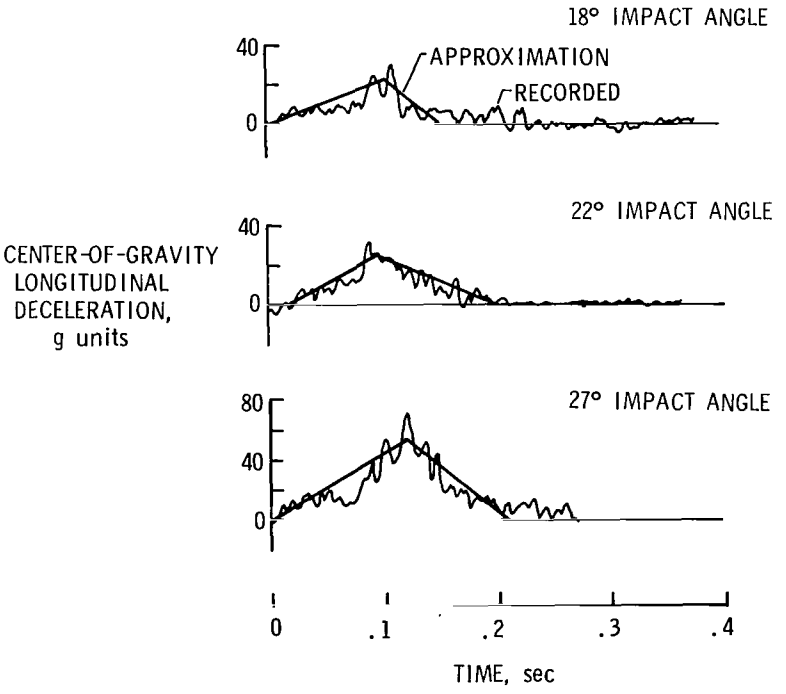

(b) Fighter airplane.

Figure 7.- Typical time histories of normal and longitudinal decelerations of transport and fighter airplanes.

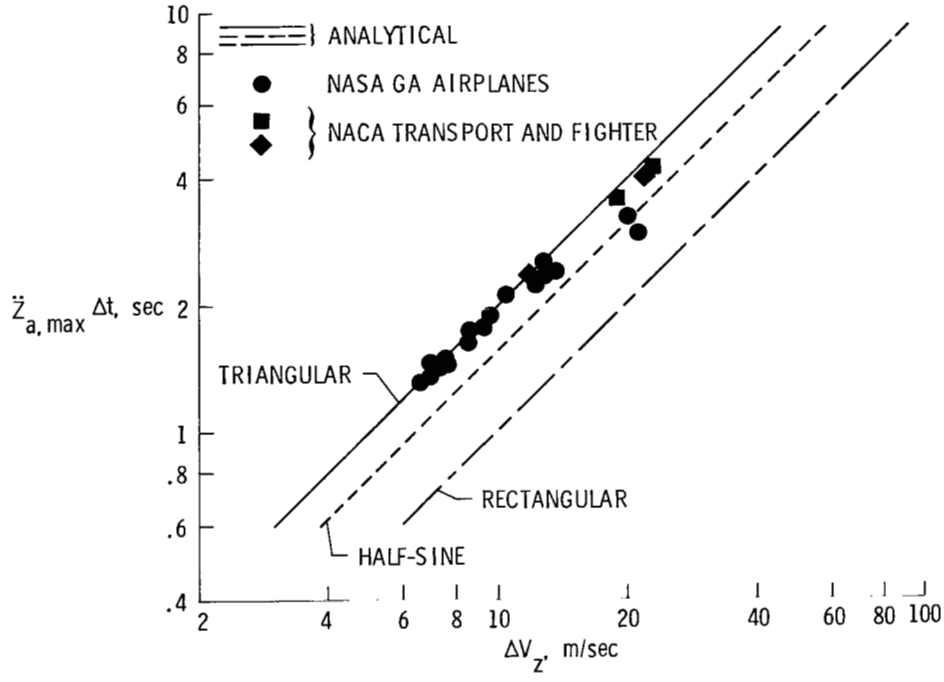

Figure 8.- Correlation of crash data with flight parameters at impact in airplane normal axis direction.

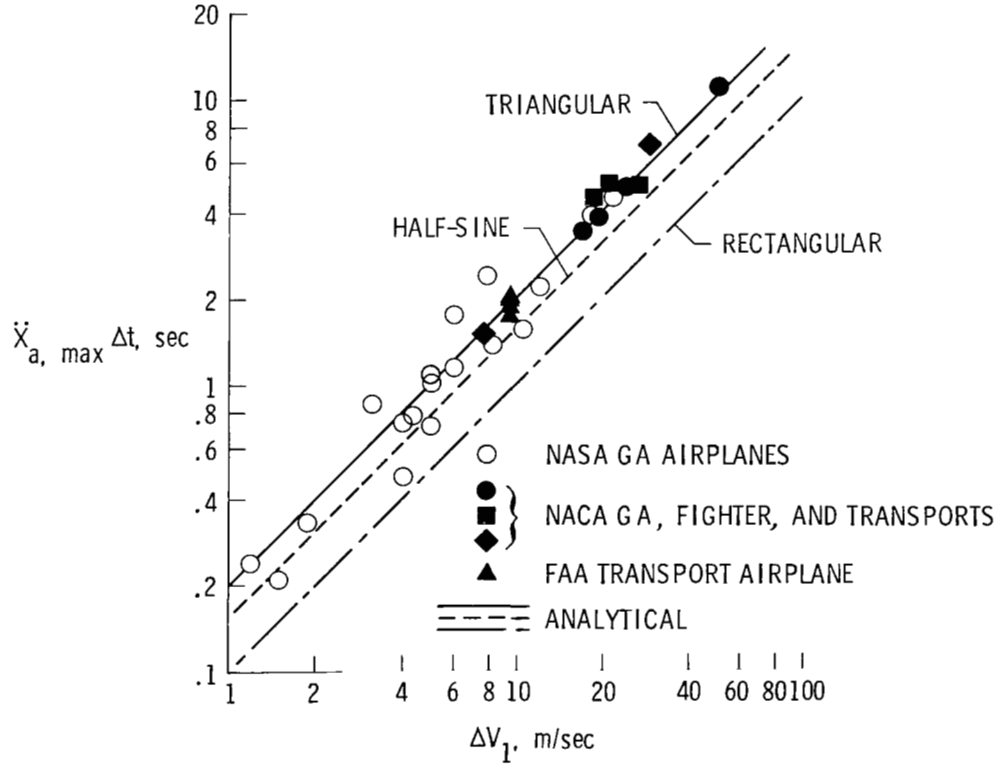

Figure 9.- Correlation of crash data with flight parameters at impact in airplane longitudinal axis direction.

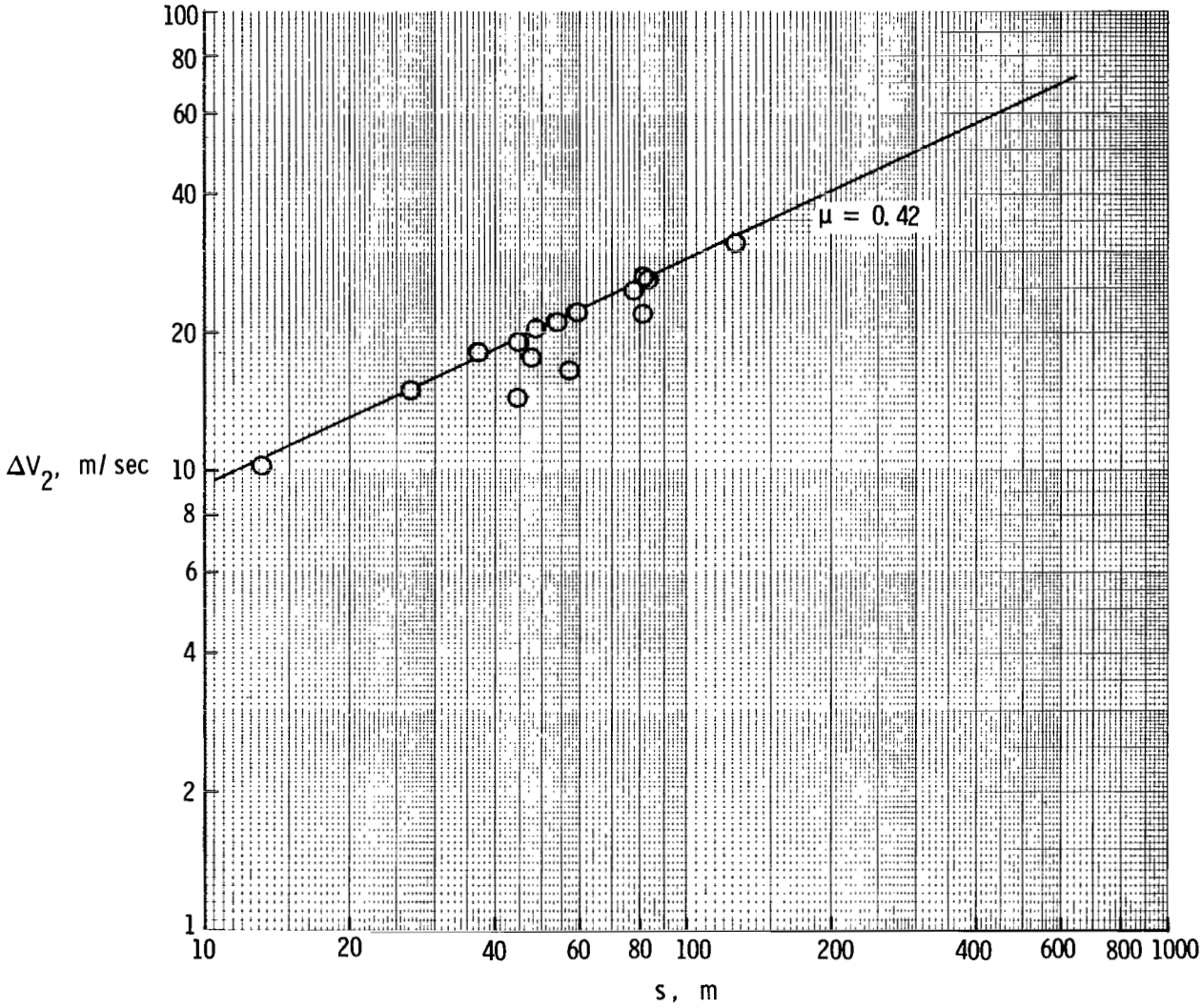

Figure 10.- Velocity change during slide-out versus slide-out distance.

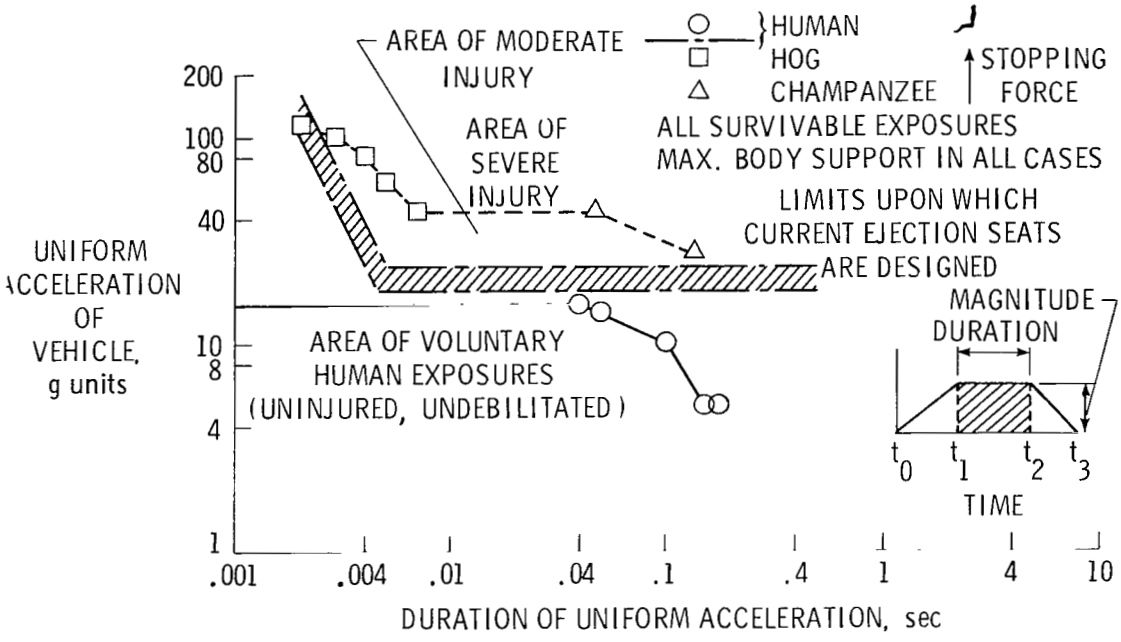

Figure 11.- Eiband curves for human tolerance.

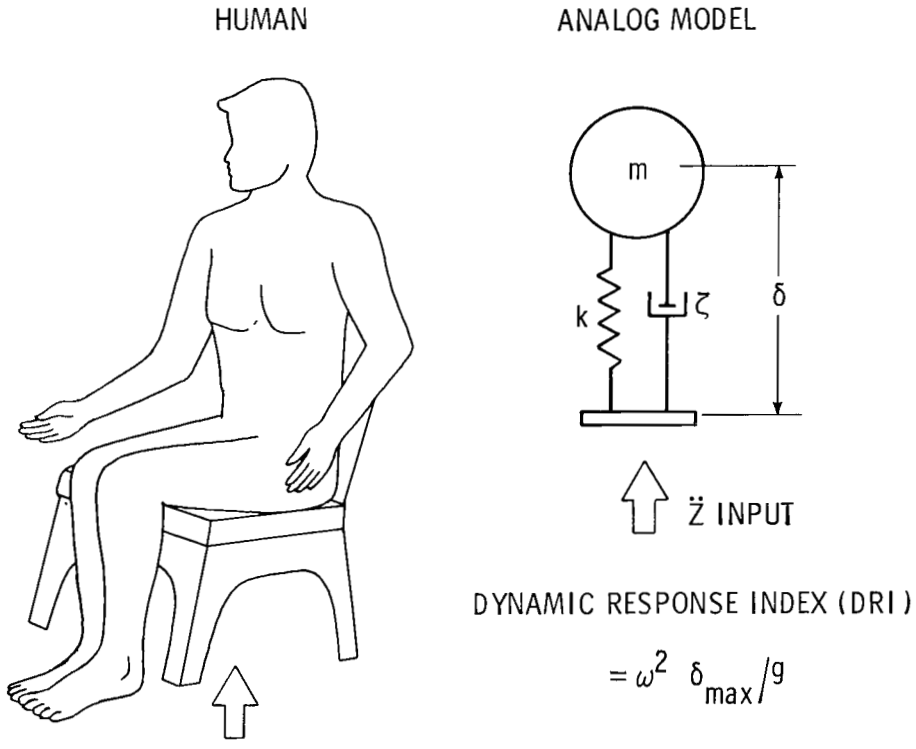

Figure 12.- Dynamic Response Index (DRI) model.

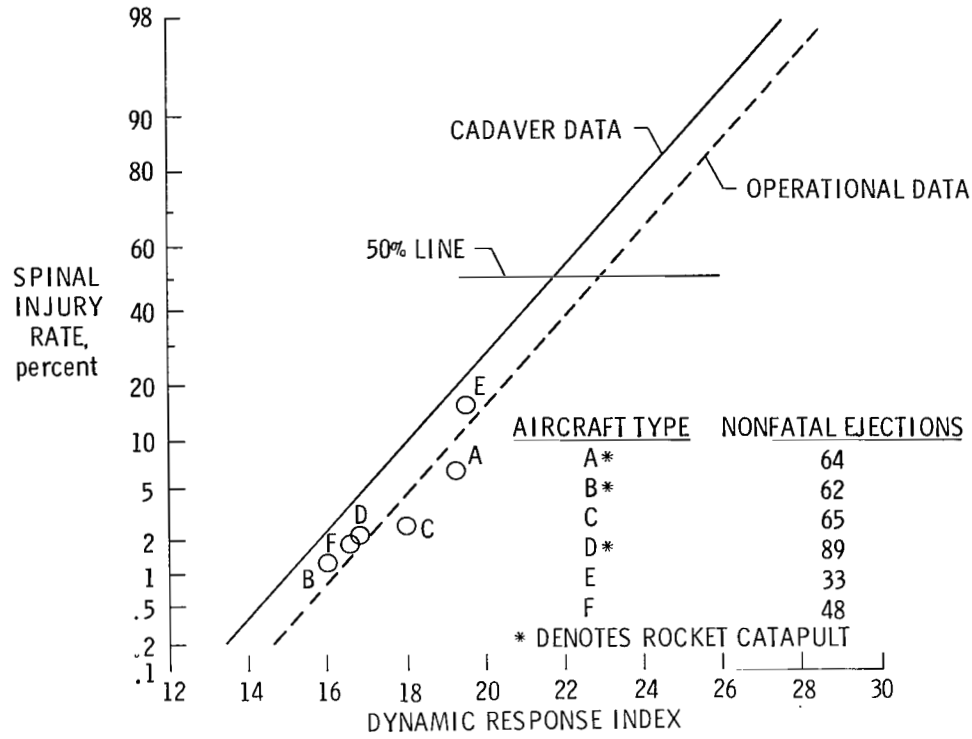

Figure 13.- Spinal injury rate as a function of dynamic response index.

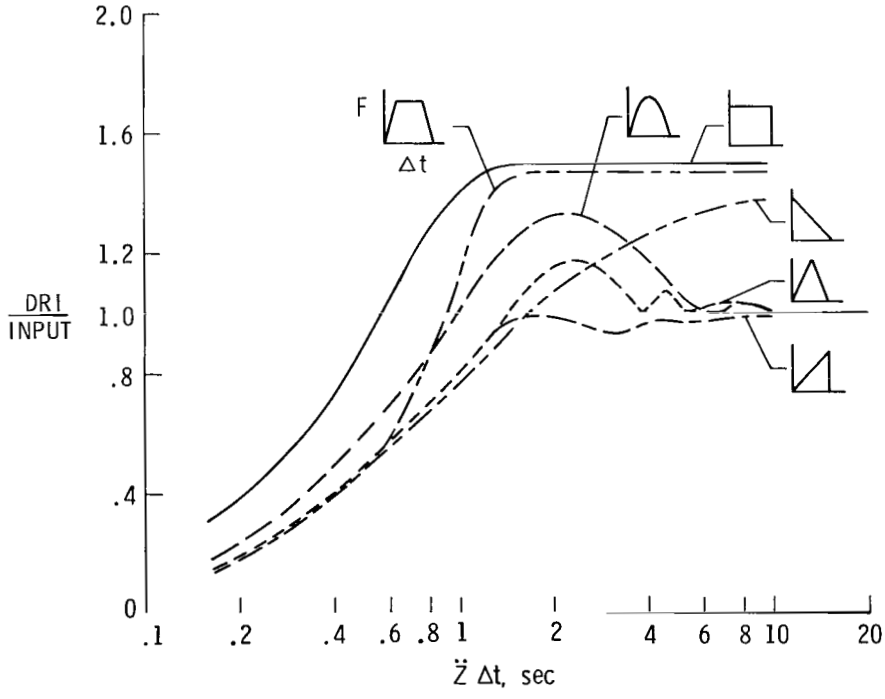

Figure 14.- DRI-impulse data for various pulse shapes.

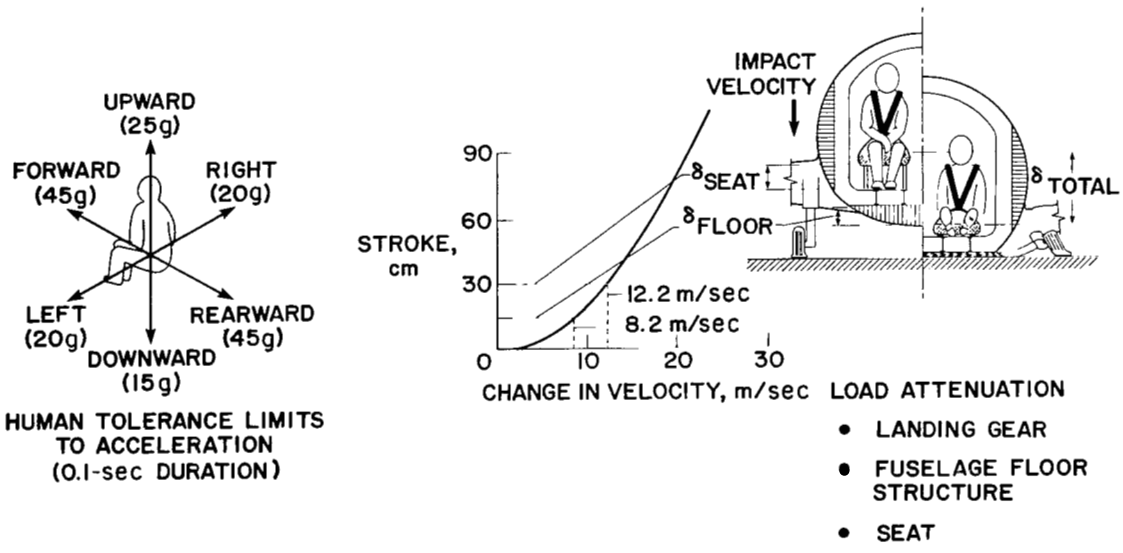

Figure 15.- Stroke as a function of velocity change in typical twin-engine general aviation airplanes.

(a) Exterior view of crashed airplane.

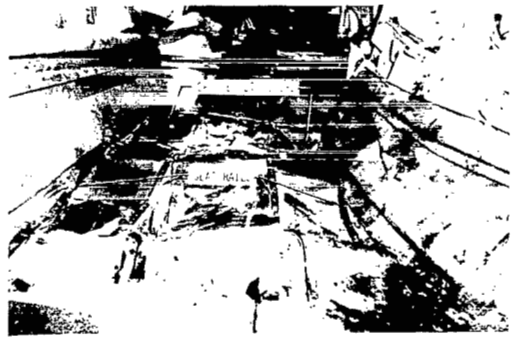

(b) Cabin floor of crashed airplane (seats removed).

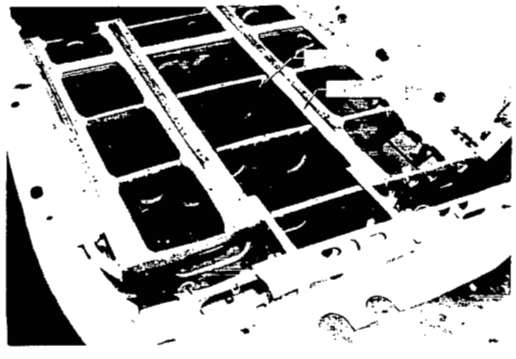

(c) Airplane section showing floor beams and bulkheads.

L-84-30

Figure 16.- Field accident data on subfloor behavior for a twin-engine airplane.

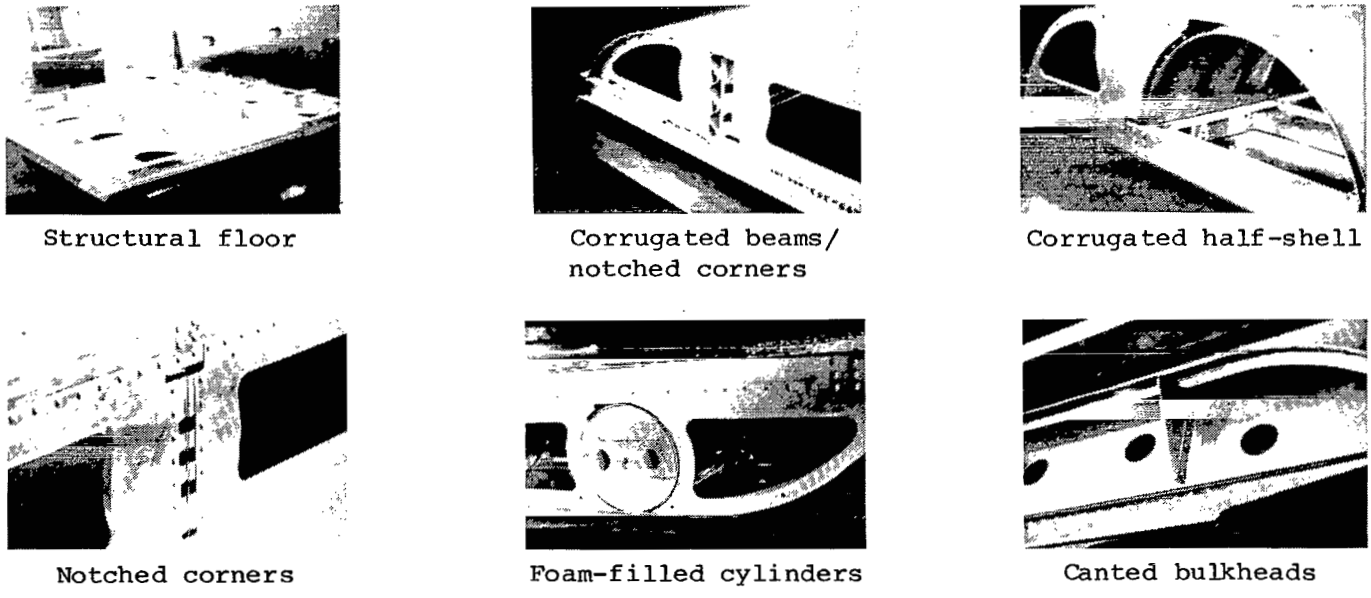

Figure 17.- Load-limiting airplane subfloor concepts.

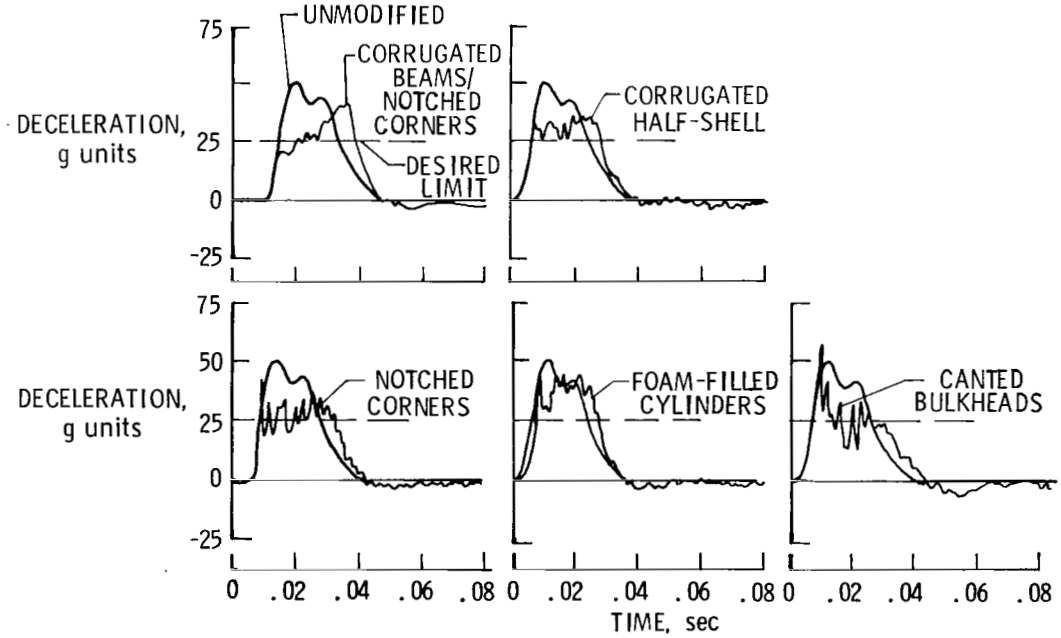

Figure 18.- Summary of unmodified and load-limiting subfloor responses. Lead mass c.g.

L-81-10,041

Figure 19.- Full-scale airplane subfloor modification using notched corners and corrugated beams.

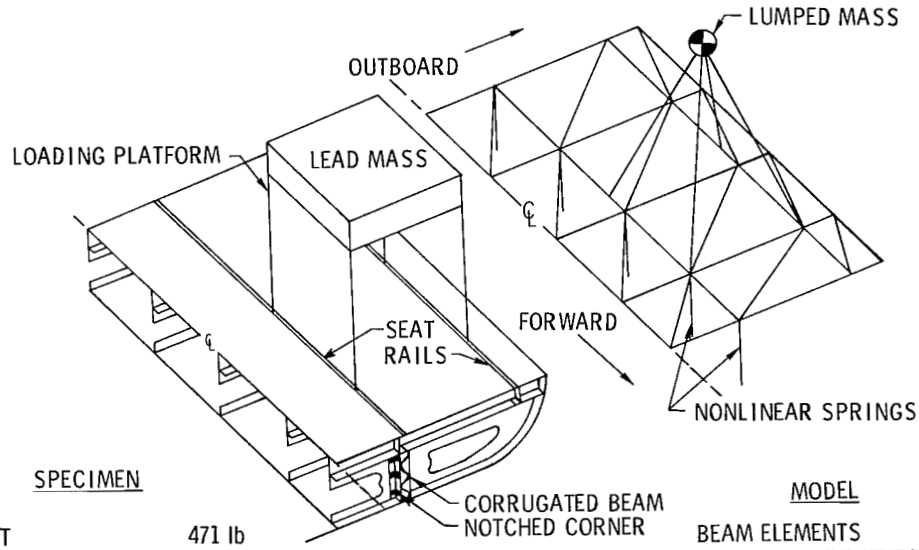

SPECIMEN	
WEIGHT	471 lb
VERTICAL VELOCITY	24 ft/sec

MODEL	
BEAM ELEMENTS	40
MEMBRANE ELEMENTS	24
NONLINEAR SPRINGS	5
DOF	39
CYBER 175	8.1 sec/msec
TIME STEP	10^{-6} to 10^{-4} sec

Figure 20.- Typical subfloor idealization using DYCAST analysis.

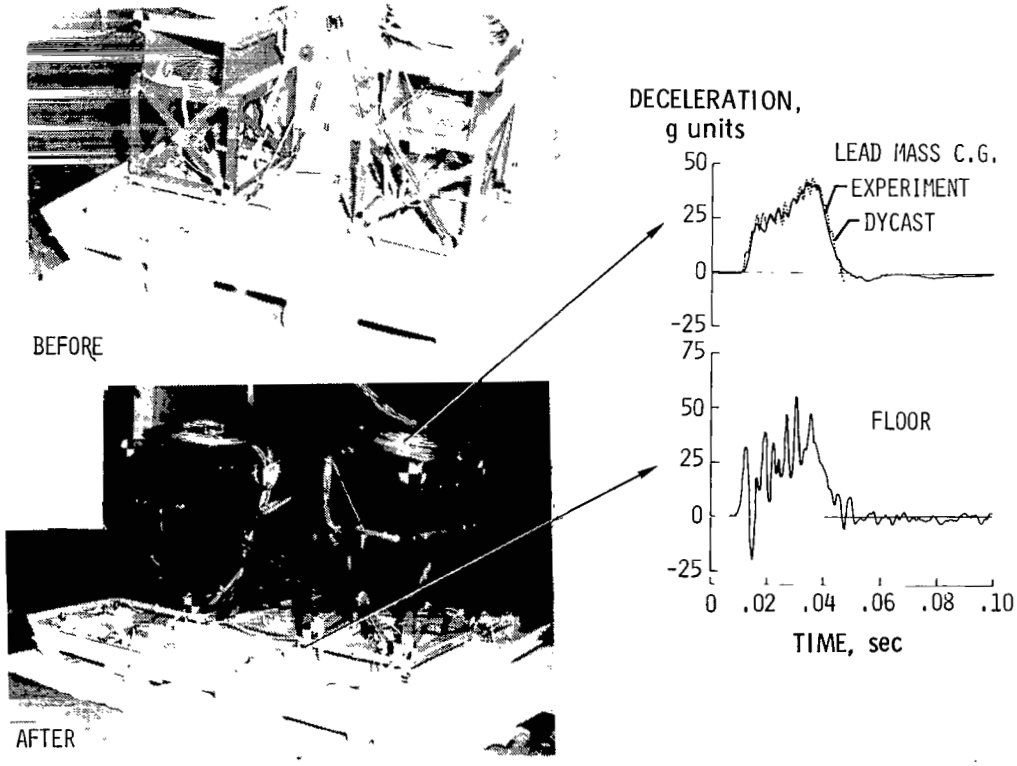

L-84-32

Figure 21.- Analytical and experimental impact results for corrugated beams with notched corners subfloor.

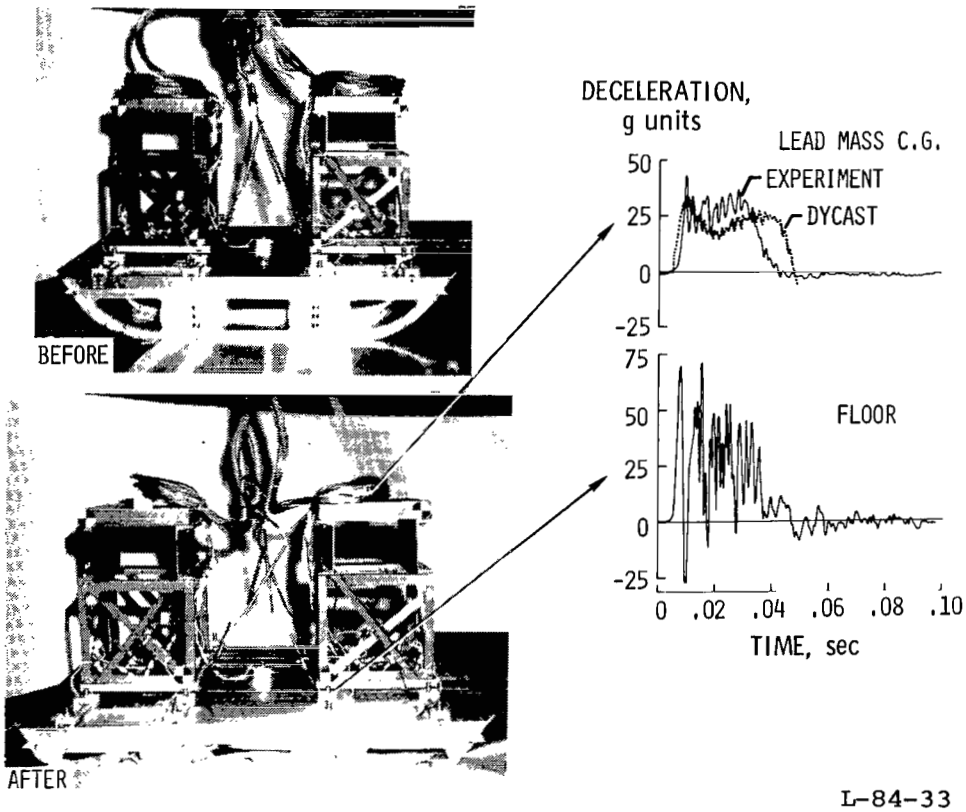

L-84-33

Figure 22.- Analytical and experimental impact results for notched corners subfloor.

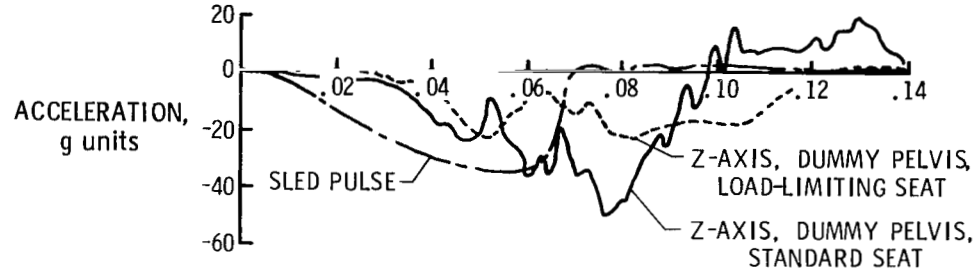

L-84-34

(a) "Vertical"; Pitch angle, -30°; roll angle, 10°.

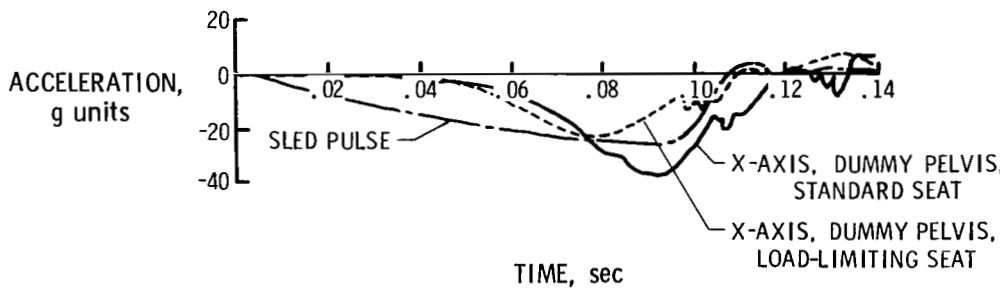

L-84-35

(b) "Longitudinal"; 30° yaw.

Figure 23.- Pelvis accelerations for dummy in standard and load-limiting seats subjected to "vertical" and "longitudinal" sled pulses.

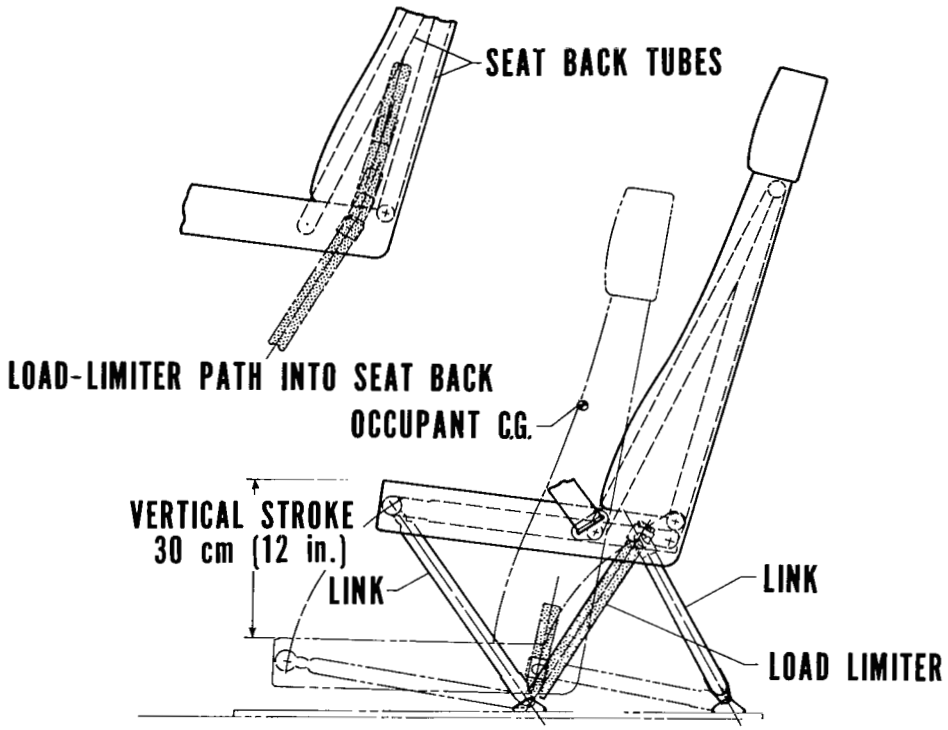

Figure 24.- Load-limiting seat mounted on floor.

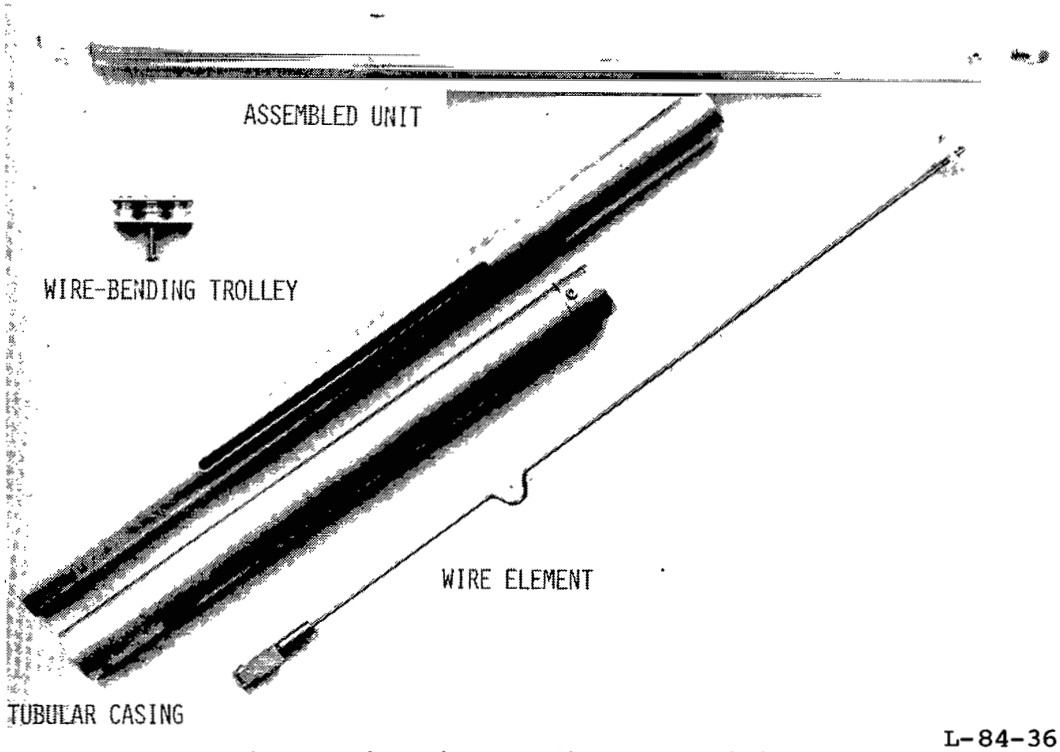

L-84-36

Figure 25.- Wire-bending load limiter.

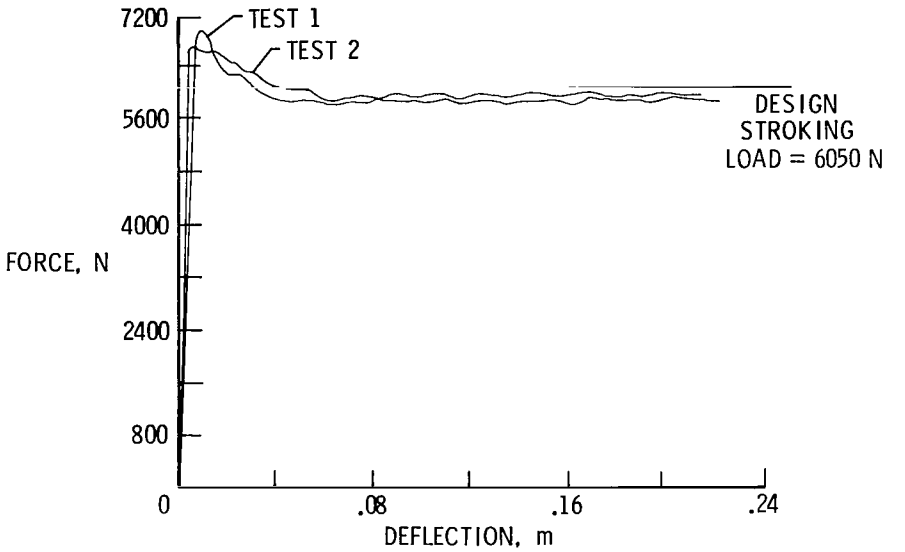

Figure 26.- Wire-bending load-deflection characteristics.

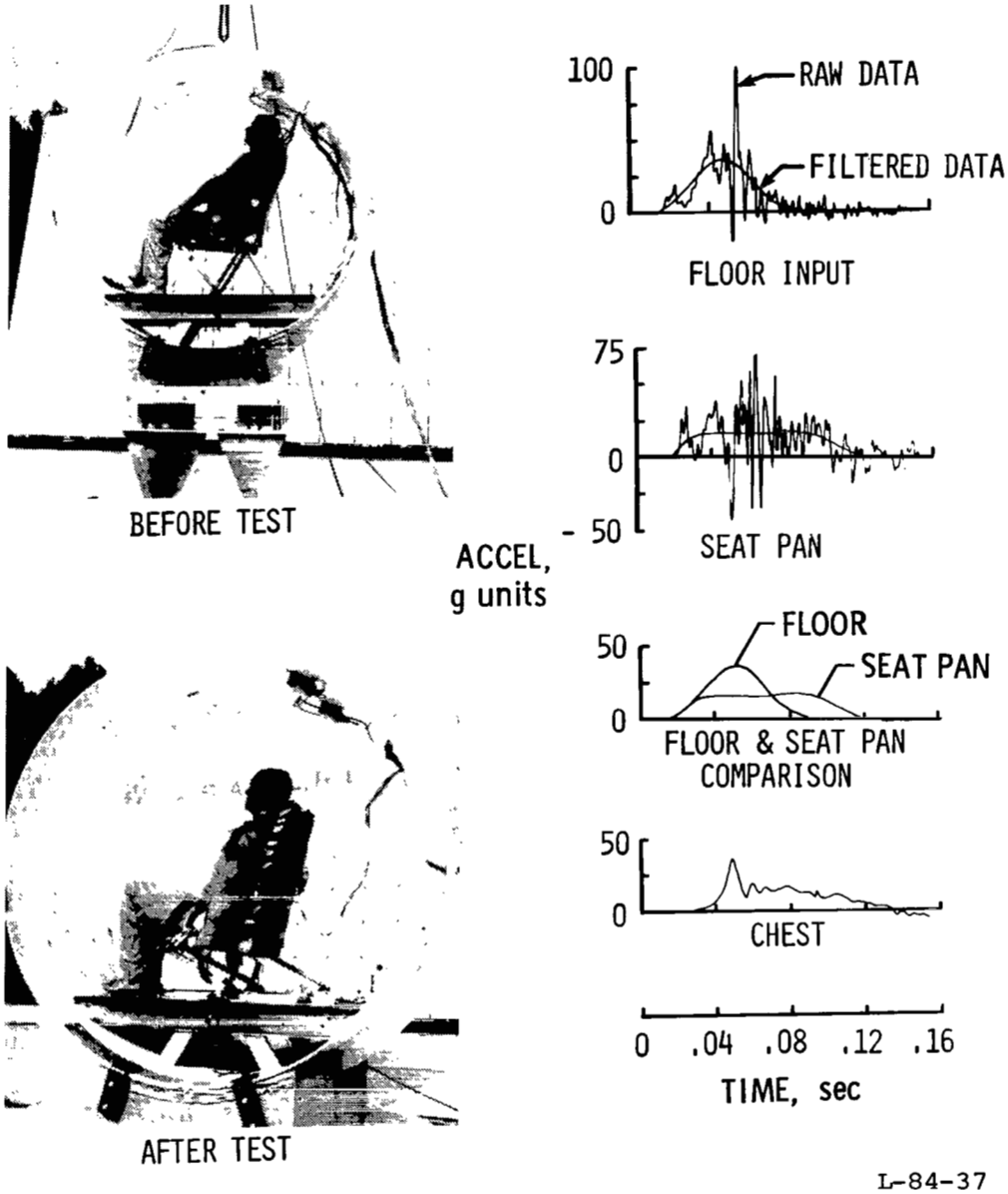

Figure 27.- Vertical drop test at 0° pitch angle.

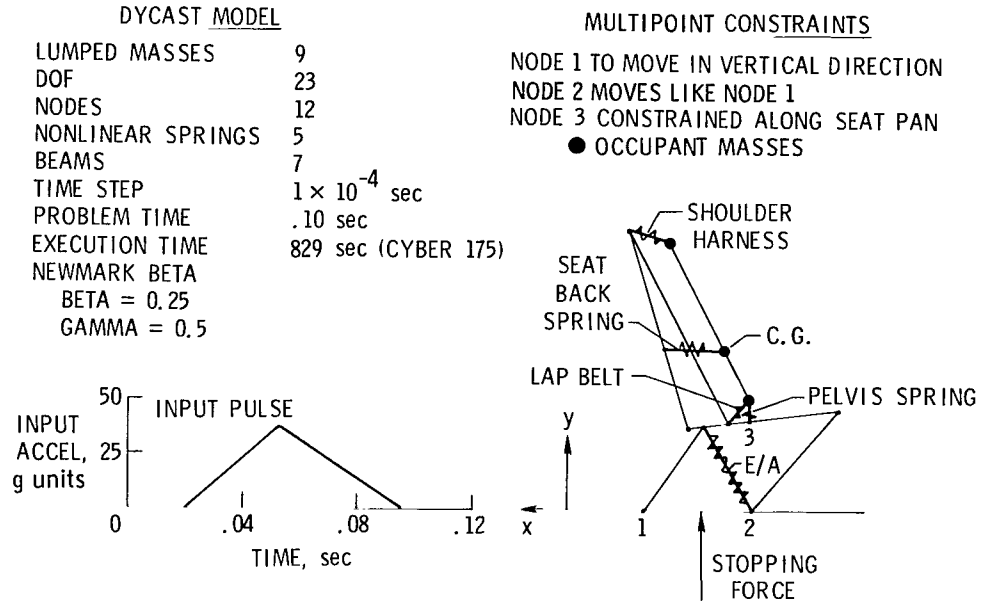

Figure 28.- DYCAST model for floor-mounted load-limiting seat.

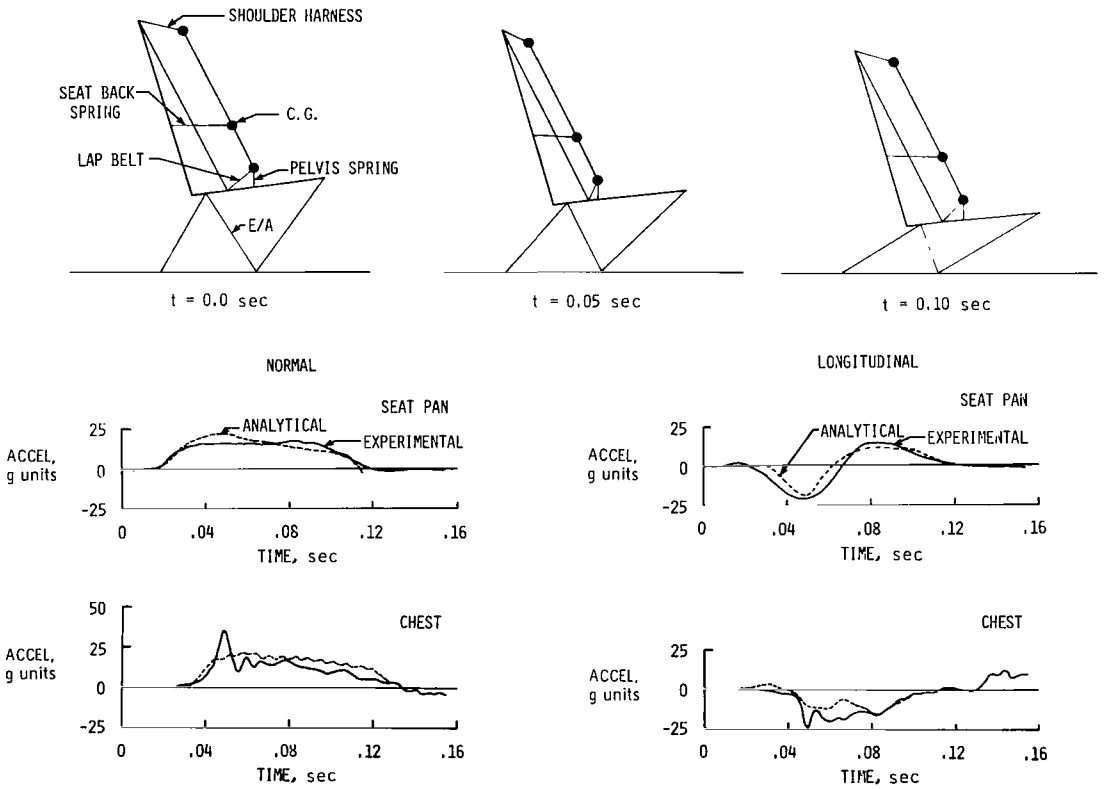

Figure 29.- Comparison of accelerations predicted by DYCAST model with vertical drop data at 0° pitch angle.

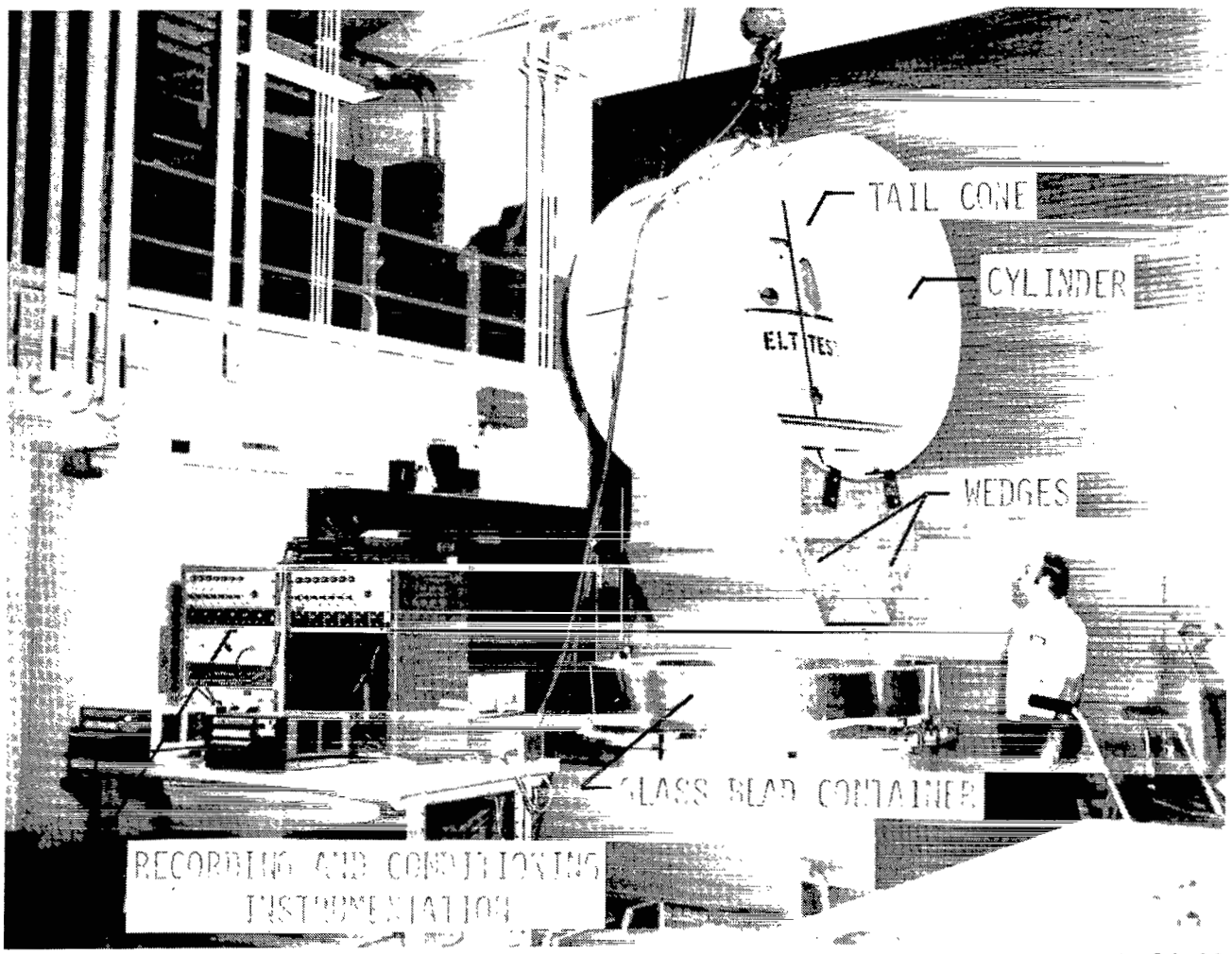

L-84-38

Figure 30.- Emergency Locator Transmitter (ELT) test apparatus.

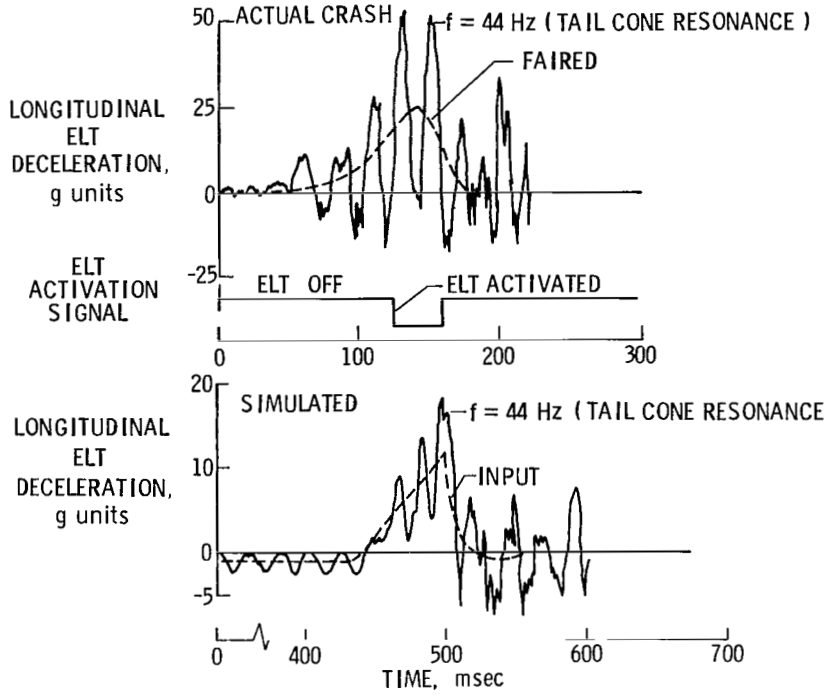

Figure 31.- Actual and simulated longitudinal crash pulses subjected to ELT's.

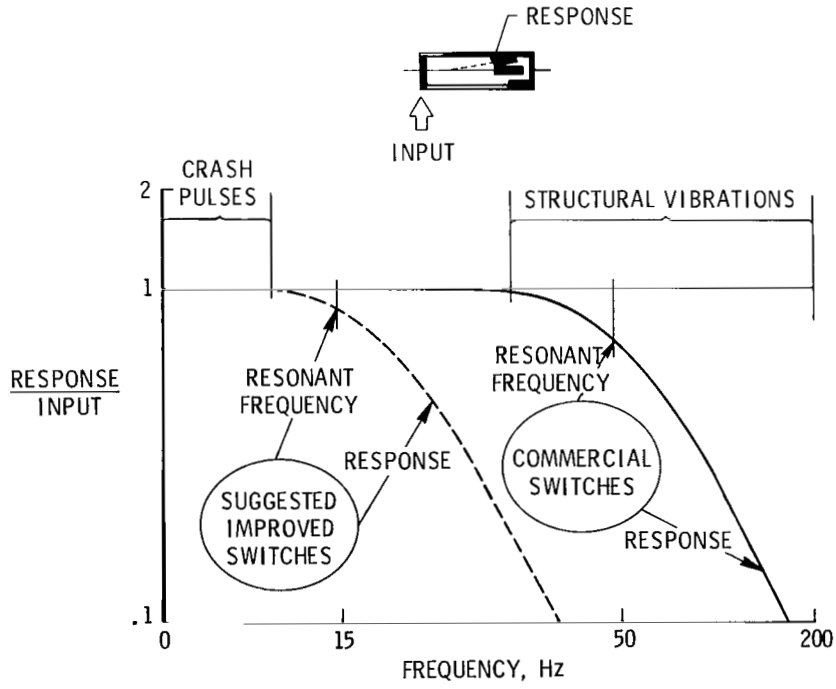

Figure 32.- Input and response frequency domains for ELT's.

1. Report No.	2. Government Accession No.	3. Recipient's Catalog No.
NASA TP-2298		

4. Title and Subtitle	5. Report Date
SURVEY OF NASA RESEARCH ON CRASH DYNAMICS	April 1984
	6. Performing Organization Code: 505-33-53-05
7. Author(s): Robert G. Thomson, Huey D. Carden, and Robert J. Hayduk	8. Performing Organization Report No.: L-15757
	10. Work Unit No.
9. Performing Organization Name and Address: NASA Langley Research Center, Hampton, VA 23665	11. Contract or Grant No.
	13. Type of Report and Period Covered: Technical Paper
12. Sponsoring Agency Name and Address: National Aeronautics and Space Administration, Washington, DC 20546	14. Sponsoring Agency Code

15. Supplementary Notes

16. Abstract

Ten years of structural crash dynamics research activities conducted on general aviation aircraft by the National Aeronautics and Space Administration (NASA) are described. Thirty-two full-scale crash tests were performed at Langley Research Center, and pertinent data on airframe and seat behavior were obtained. Concurrent with the experimental program, analytical methods were developed to help predict structural behavior during impact. In this paper, there is an assessment of the effects of flight parameters at impact on cabin deceleration pulses at the seat/occupant interface, experimental and analytical correlation of data on load-limiting subfloor and seat configurations, airplane section test results for computer modeling validation, and data from emergency-locator-transmitter (ELT) investigations to determine probable cause of false alarms and nonactivations. Computer programs which can provide designers with analytical methods for predicting accelerations, velocities, and displacements of collapsing structures are also discussed.

17. Key Words (Suggested by Author(s))	18. Distribution Statement
Emergency locator transmitter Airplane crash tests Load-limiting subfloors Load-limiting seats Crash damage General aviation Impact tests Crash dynamics Impulse analysis	Unclassified - Unlimited Subject Category 39

19. Security Classif. (of this report)	20. Security Classif. (of this page)	21. No. of Pages	22. Price
Unclassified	Unclassified	44	A03

For sale by the National Technical Information Service, Springfield, Virginia 22161 NASA-Langley, 1984

National Aeronautics and
Space Administration

Washington, D.C.
20546

Official Business
Penalty for Private Use, $300

THIRD-CLASS BULK RATE

Postage and Fees Paid
National Aeronautics and
Space Administration
NASA-451

U.S.MAIL

1 1 1U,D, 840417 S00903DS
DEPT OF THE AIR FORCE
AF WEAPONS LABORATORY
ATTN: TECHNICAL LIBRARY (SUL)
KIRTLAND AFB NM 87116

NASA

POSTMASTER: If Undeliverable (Section 158
Postal Manual) Do Not Return